Geochemistry Geophysics Geosystems G3

Article
Volume 11, Number 12
15 December 2010
Q12S29, doi:10.1029/2010GC003273
ISSN: 1525-2027

Published by AGU and the Geochemical Society

Thermal regime of the Costa Rican convergent margin: 2. Thermal models of the shallow Middle America subduction zone offshore Costa Rica

Robert N. Harris
College of Oceanic and Atmospheric Sciences, Oregon State University, Corvallis, Oregon 97331, USA (rharris@coas.oregonstate.edu)

Glenn Spinelli
Department of Earth and Environmental Sciences, New Mexico Institute of Mining and Technology, Socorro, New Mexico 87801, USA

César R. Ranero
Barcelona Center for Subsurface Imaging, ICREA, Instituto de Ciencias del Mar, CSIC, Pg. Marítim de la Barcelona 37-49, E-08003 Barcelona, Spain

Ingo Grevemeyer
Leibniz Institute of Marine Sciences at University of Kiel (IFM-GEOMAR), D-24148 Kiel, Germany

Heinrich Villinger
Department of Geosciences, University of Bremen, PO Box 330 440, D-28334 Bremen, Germany

Udo Barckhausen
Federal Institute for Geosciences and Natural Resources, Stilleweg 2, D-30655 Hannover, Germany

[1] At the Costa Rica margin along the Middle America Trench along-strike variations in heat flow are well mapped. These variations can be understood in terms of either ventilated fluid flow, where exposed basement allows fluids to freely advect heat between the crustal aquifer and ocean, or insulated fluid flow where continuous sediment cover restricts heat advection to within the crustal aquifer. We model fluid flow within the subducting aquifer using Nusselt number approximations coupled with finite element models of subduction and explore its effect on temperatures along the subduction thrust. The sensitivity of these models to the initial thermal state of the plate and styles of fluid flow, either ventilated or insulated, is explored. Heat flow measurements on cool crust accreted at the East Pacific Rise are consistent with ventilated hydrothermal cooling that continues with subduction. These models yield much cooler temperatures than predicted from simulations initialized with conductive predictions and without hydrothermal circulation. Heat flow transects on warm crust accreted at the Cocos-Nazca spreading center are consistent with models of insulated hydrothermal circulation that advects heat updip within the subducting crustal aquifer. Near the trench these models are warmer than conductive predictions and cooler than conductive predictions downdip of the trench. Comparisons between microseismicity and modeled isotherms suggest that the updip limit of microseismicity occurs at temperatures warmer than 100°C and that the downdip extent of microseismicity is bounded by the intersection of the subduction thrust with the base of the overriding crust.

Components: 13,200 words, 9 figures, 3 tables.

Keywords: subduction zones; thermal model; fluid flow.

Index Terms: 3060 Marine Geology and Geophysics: Subduction zone processes (1031, 3613, 8170, 8413); 3015 Marine Geology and Geophysics: Heat flow (benthic); 3017 Marine Geology and Geophysics: Hydrothermal systems (0450, 1034, 3616, 4832, 8135, 8424).

Received 22 June 2010; **Revised** 14 October 2010; **Accepted** 20 October 2010; **Published** 15 December 2010.

Harris, R. N., G. Spinelli, C. R. Ranero, I. Grevemeyer, H. Villinger, and U. Barckhausen (2010), Thermal regime of the Costa Rican convergent margin: 2. Thermal models of the shallow Middle America subduction zone offshore Costa Rica, *Geochem. Geophys. Geosyst.*, *11*, Q12S29, doi:10.1029/2010GC003273.

Theme: Central American Subduction System
Guest Editors: G. Alvarado, K. Hoernle, and E. Silver

1. Introduction

[2] A major endeavor over the past decade has focused on understanding processes influencing the location and width of the seismogenic portion of the subduction thrust [e.g., *Dixon and Moore*, 2007]. The subduction thrust accommodates slip between subducting and overriding plates, and its seismogenic portion is defined as the region where large earthquakes nucleate and rupture. The seismogenic zone is characterized by regions of interseismic locking and coseismic slip. Understanding seismogenic transitions at the updip and downdip limits is important for understanding processes associated with earthquakes and tsunamis. Updip and downdip of the seismogenic zone, changing frictional conditions and high fluid pressures likely facilitate aseismic slip [e.g., *Peng and Gomberg*, 2010]. However, a range of slip behavior along the subduction thrust is now recognized such that transitions limiting the seismogenic zone are spatially and temporally more complicated than previously thought [e.g., *Schwartz and Rokosky*, 2007].

[3] The width of the seismic zone spans a limited range of temperatures (see summary by *Oleskevich et al.* [1999]). The downdip extent of observed seismicity is approximately correlated with the 350°C isotherm or the intersection of the overriding Moho with the subduction thrust, whichever is shallower. This correlation is understood in terms of either the brittle-ductile transition or the intersection of the subduction thrust with hydrated mantle [*Hyndman et al.*, 1997; *Peacock and Hyndman*, 1999; *Seno*, 2005], but is complicated by the limited accuracy of hypocenter depth determinations, the depth of the Moho and thermal models of subduction [*Oleskevich et al.*, 1999]. The updip extent of observed seismicity appears well correlated with temperatures in the 100°C–150°C range [*Hyndman and Wang*, 1993; *Hyndman et al.*, 1997; *Oleskevich et al.*, 1999; *Currie et al.*, 2002; *Harris and Wang*, 2002; *Spinelli and Saffer*, 2004]. These correlations support the hypothesis that temperature exerts a primary influence on the updip and downdip boundaries of the seismogenic zone. The updip frictional transition likely reflects the complex interplay of temperature-dependent processes with the composition, thickness, and progressive lithification of incoming sediment, the concentration of interstitial and bound water being subducted, and basement relief [*Hyndman and Wang*, 1993; *Moore and Saffer*, 2001; *Underwood*, 2007; *Bilek et al.*, 2003; *Lay and Bilek*, 2007; *Marone and Saffer*, 2007; *Schwartz and DeShon*, 2007; *Ranero et al.*, 2008].

[4] *Harris et al.* [2010] determine values of heat flow along multiple transects from geothermal probe measurements and from bottom-simulating reflectors (BSRs) and generate a regional thermal map of the margin. Collocated geothermal probe and BSR values of heat flow are well correlated. This correlation improves with distance landward from the trench implying that in regions where BSRs are present conductive heat transfer generally characterizes the shallow margin. In other areas high wave number variations in heat flow are interpreted in terms of advective fluid flow through normal faults penetrating the margin, slumping, and deformation.

[5] In this study we use the heat flow results from *Harris et al.* [2010] to constrain thermal models of the Middle America subduction zone. This convergent margin is an important area to investigate relationships between temperature and seismicity

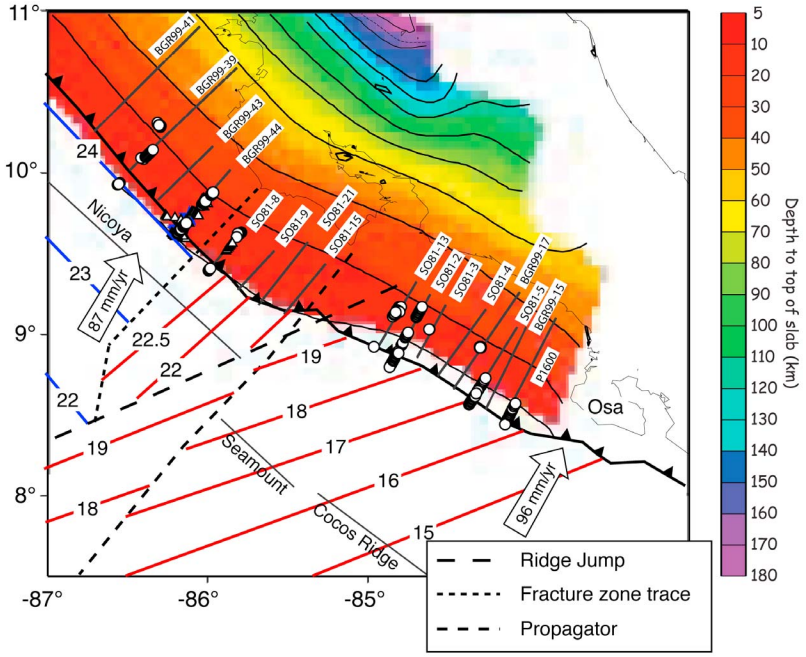

Figure 1. Tectonic setting of the Middle America Trench showing magnetic lineations and age of incoming oceanic crust in Myr. Magnetic lineations on crust formed at the East Pacific Rise and those formed at the Cocos-Nazca Spreading Center are shown in blue and red, respectively. This boundary is known as the plate suture. The crust has been divided into three segments based on its morphological characteristics: the Nicoya, Seamount, and Cocos Ridge segments [*von Huene et al.*, 1995]. Color contours show the shape of the descending plate [*Ranero et al.*, 2005]. The contour interval is 20 km. The positions of seismic reflection profiles are shown as solid lines, and heat flow data described by *Harris et al.* [2010] are shown as white circles. Heat flow data from *Langseth and Silver* [1996] are shown as white triangles.

because of a good distribution of along-strike heat flow observations [*Harris et al.*, 2010] and well-mapped seismicity [*DeShon et al.*, 2003, 2006; *Ghosh et al.*, 2008]. The focus of this study is on low wave number variations and on along-strike variations in the shallow subduction zone where surface observations of heat flow are most sensitive to subduction thrust temperatures. We start by reviewing components of the tectonic setting that help control the thermal structure of the subduction zone, and then review regional heat flow data that provide insight into the thermal regime of the incoming plate. These reviews are used to guide the development of subduction zone thermal models in which we pay particular attention to the initial geotherm and the effects of hydrothermal circulation. We then explore the sensitivity of our simulations to realistic variations in model parameters and compare these simulations with heat flow data presented by *Harris et al.* [2010]. Finally, we present a thermal model based on our preferred set of model parameters and discuss the implications of this model within the context of the seismogenic zone.

2. Tectonic Setting

[6] The Middle America Trench (MAT) delineates the position where the Cocos plate subducts beneath the Caribbean plate (Figure 1). The overriding Costa Rican Isthmus is composed of Mesozoic and Cenozoic thickened oceanic crust thought to be part of the Caribbean Large Igneous Province [e.g., *Pindell and Barrett*, 1990; *Sinton et al.*, 1997]. This crust has a regional thickness of about 40 km, but thins to about 30 km at the Nicoya Peninsula [*Sallarès et al.*, 2001; *MacKenzie et al.*, 2008]. Along-strike variations in the incoming oceanic plate from north to south include plate age, convergence rate, seafloor relief, and subduction dip.

[7] Magnetic lineations indicate that the oceanic crust ranges in age from 24 Ma offshore northern Costa Rica to 15–16 Ma offshore southern Costa

Rica [*Barckhausen et al.*, 2001]. An abrupt change in orientation of these magnetic lineations offshore the Nicoya Peninsula marks the boundary between crust accreted at the fast spreading rate East Pacific Rise (EPR) and crust accreted at the intermediate spreading rate Cocos Nazca Spreading Center (CNS) [*Barckhausen et al.*, 2001]. This boundary is known as the plate suture. The convergence rate between the Cocos and Caribbean plates is generally high, increasing from 87 mm/yr offshore the northern Nicoya Peninsula to 96 mm/yr offshore the Osa Peninsula [*DeMets*, 2001]. Within our study area, the azimuth of subduction varies between approximately 20° and 30° from normal along strike [*DeMets*, 2001].

[8] EPR generated seafloor, north of the plate suture, has a generally thicker sediment cover and is generally smoother than CNS generated seafloor [*von Huene et al.*, 1995; *Protti et al.*, 1995]. The rougher seafloor relief associated with CNS crust is due to its interaction with the Galapagos hot spot [*Hey*, 1977] manifested as an increase in seamount occurrence, plateaus and linear ridges.

[9] In general the morphology of the trench and plate curvature reflects a combination of an increasingly younger and thicker crust to the south. Offshore northern Costa Rica the plate is characterized by relatively large curvature and well-developed plate bending normal faults with large offsets [*Ranero et al.*, 2003, 2005]. With distance to the south this character changes to a poorly developed trench, and a decrease in observed plate-bending normal faults. Offshore the Osa Peninsula, where the Cocos Ridge subducts, undisturbed sediments overlie fault blocks suggesting that observed faults are old and unrelated to subduction [*Ranero et al.*, 2005].

[10] The shallow margin structure of Costa Rica is well characterized by seismic reflection and refraction data [*Hinz et al.*, 1996; *Ye et al.*, 1996; *Stavenhagen et al.*, 1998; *Christeson et al.*, 1999; *Sallarès et al.*, 2000; *von Huene et al.*, 2000; *Ranero and von Huene*, 2000; *Ranero et al.*, 2007, 2008]. At greater depths, the margin structure and plate interface location are constrained by earthquake locations and seismic tomography [*Husen et al.*, 2003; *DeShon et al.*, 2003, 2006; *Ghosh et al.*, 2008; *Syracuse et al.*, 2008].

[11] In general, the dip of the subducting plate increases with distance landward from the trench and decreases from north to south along the Costa Rican margin (Figure 1). Offshore the Nicoya Peninsula, the dip of the subducting EPR crust increases from ~6° near the trench to approximately 35° by a distance of approximately 90 km from the trench [*Christeson et al.*, 1999]. Inversions of P wave arrival time and S-P travel time delays recorded by a temporary array of on land and offshore seismometers show that the change in subduction dip across the plate suture is less dramatic than previously thought, but still resolves a decrease in the dip angle from north to south [*DeShon et al.*, 2006]. South of the Nicoya Peninsula, crustal thickness increases to a maximum of 10–12 km associated with the Cocos Ridge [*Walther*, 2003], and age decreases leading to a more buoyant plate that results in a relatively shallow dip. In this region aftershock events indicate the Cocos Plate has a dip of approximately 19° [*Stavenhagen et al.*, 1998; *DeShon et al.*, 2003]. Because the dip of the subduction thrust at these greater depths is based on many hypocenter locations, the dip is likely accurate within 10% or less. For depths of about 70 to 200 km, the depth to the top of the slab is imaged by both regional earthquakes and the global EHB catalog [*Engdahl et al.*, 1998] and from global tomography as indicated by *Ranero et al.* [2005].

[12] Overall the generally decreasing plate age and slab dip to the south can be expected to lead to a warmer subduction system. This trend is counteracted to some extent by the increasing convergence rate to the south. But as described later, these effects are strongly modified by the thermal regime of the incoming plate and hydrothermal circulation.

3. Regional Heat Flow

[13] Values of surface heat flow vary greatly offshore Costa Rica and have important implications for the thermal state of the Cocos plate at the MAT. A series of regional heat flow measurements reveal a large along-strike variation in heat flow (Figure 2) [*Von Herzen and Uyeda*, 1963; *Vacquier et al.*, 1967]. Despite lacking high-quality bathymetric and seismic information that permit detailed interpretation, these measurements indicate that EPR-generated seafloor of the Cocos Plate has low heat flow relative to the global mean for crust of the same age. The mean value and standard deviation of regional heat flow data on EPR seafloor are approximately 30 and 15 mW m^{-2}, respectively. For seafloor of this age, conductive predictions are ~100–130 mW m^{-2} [*Stein and Stein*, 1992]. In contrast, heat flow values on CNS-generated seafloor are close to the conductive prediction but above the global mean for crust of this age. These

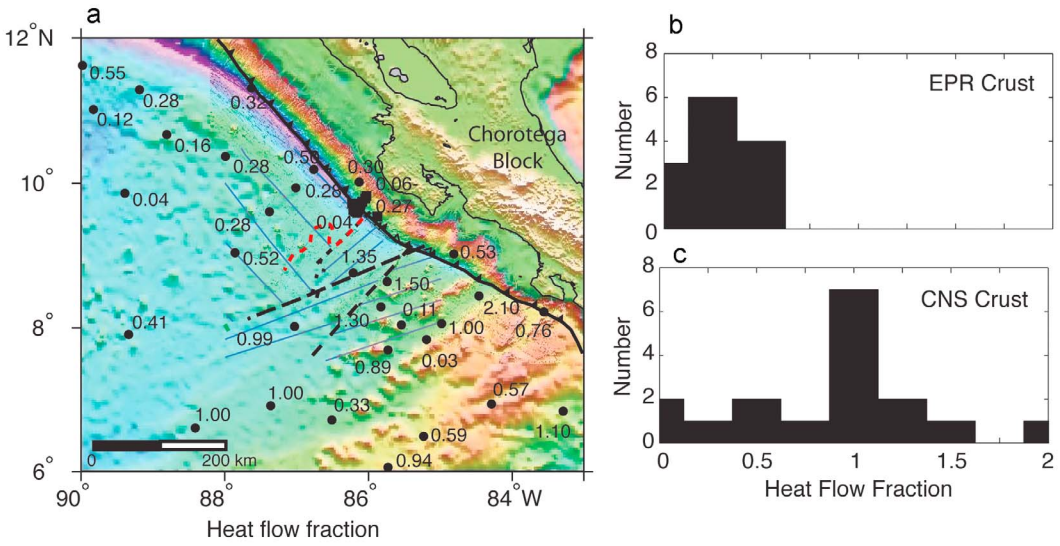

Figure 2. Regional heat flow offshore Costa Rica [*Von Herzen and Uyeda*, 1963; *Vacquier et al.*, 1967]. (a) Map of regional heat flow showing heat flow fraction calculated as the ratio of observed to predicted heat flow based on the GDH1 model [*Stein and Stein*, 1992]. The dashed red line shows transition between warm and cool crust [*Fisher et al.*, 2003]. Dashed black lines show the locations of the ridge jump, fracture zone trace, and propagator as defined in Figure 1. Magnetic lineations on crust formed at the East Pacific Rise and those formed at the Cocos-Nazca Spreading Center are shown in blue and red, respectively. This boundary is known as the plate suture. (b) Histogram of heat flow fraction north of the plate suture. This seafloor was accreted at the East Pacific Rise (EPR). (c) Histogram of heat flow fraction south of the plate suture. This crust was accreted at the Cocos-Nazca Spreading Center (CNS). Only regional heat flow values collected seaward of the Middle America Trench are used to construct the histograms.

values exhibit large variability indicative of fluid flow with a mean and standard deviation of 110 and 60 mW m^{-2}, respectively.

[14] In 2000 and 2001, heat flow studies specifically designed to investigate the nature of the thermal transition between the cold EPR and warm CNS crust were undertaken [*Fisher et al.*, 2003; *Hutnak et al.*, 2007]. Closely spaced heat flow values collocated with seismic reflection lines show a sharp transition (<5 km) between warm and cool seafloor seaward of the trench (Figure 2) indicating the transition has a shallow source consistent with fluid flow in the upper oceanic crust. Within the cool part of the survey area, heat flow values are 20–40 mW m^{-2}, consistent with previous regional values. Across the thermal transition, heat flow values are 105–115 mW m^{-2} [*Fisher et al.*, 2003; *Hutnak et al.*, 2007]. The actual boundary between warm and unusually cool values deviates from the plate suture and appears to be influenced by the proximity of basement highs that penetrate the otherwise thick sediment cover. This exposed basement on EPR accreted crust focuses discharge and efficiently ventilates the oceanic crust. Numerical models suggest basement cooling may be limited to the upper 100–600 m of basement with an effective permeability of 10^{-10}–10^{-8} m^2 [*Hutnak et al.*, 2007].

[15] In summary, heat flow observations on the incoming plate suggest the thermal regime of CNS accreted crust is broadly consistent with conductive cooling and is only locally perturbed, whereas seamounts penetrating thick sediment cover on EPR accreted crust facilitate large lateral transport of fluids that efficiently cools the crust.

[16] Heat flow profiles on the margin (Figure 1) are discussed by *Harris et al.* [2010]. These profiles show strong variations along strike consistent with regional heat flow data on the incoming Cocos Plate. Along the margin underthrust by EPR crust, heat flow is low [*Langseth and Silver*, 1996; *Fisher et al.*, 2003; *Hutnak et al.*, 2007]; along the margin under thrust by CNS crust, heat flow is generally high. The transition between the low and high heat flow correlates with the extension of the plate suture and appears relatively abrupt. High wave number variations in the heat flow data are interpreted as focused fluid flow through the margin near the deformation front. In this paper we focus on low wave number variations that we attribute to variations in the thermal structure of subduction

due to different styles of fluid flow within the subducting oceanic crust.

4. Thermal Models

[17] Previous thermal models of the shallow subduction zone in this area are based on heat flow measurements located offshore the Nicoya Peninsula in the region of ODP Leg 170. Seaward of the trench these measurements have an average of about 12 mW m^{-2} and increase to 25–30 mW m^{-2} landward of the trench [*Langseth and Silver*, 1996; *Harris et al.*, 2010]. *Langseth and Silver* [1996] modeled the margin as a deforming accretionary prism, and to match the landward increase in heat flow called on a combination of a hydrothermally perturbed geotherm that relaxed once the oceanic crust subducted and relatively high frictional heating along the subduction thrust. ODP Leg 170, however, demonstrated that the Nicoya margin is nonaccretionary [*Kimura et al.*, 1997]. *Harris and Wang* [2002] updated this model by using a nondeforming margin and calculated temperatures for the entire system. To match the landward increase in heat flow, they also used a hydrothermally perturbed geotherm as suggested by *Langseth and Silver* [1996], but found that results were consistent with a lower magnitude of frictional heating. Additionally, *Harris and Wang* [2002] showed results consistent with a standard conductive geotherm representing CNS crust on the southern side of the plate suture. This warmer scenario moves the 100°C–150°C isotherm approximately 25 km seaward. *Newman et al.* [2002] correlated observed changes in the updip limit of seismicity with the changing position of the 100°C–150°C isotherm across the thermal transition. *Spinelli and Saffer* [2004] developed a thermal model using a 1-D transient simulation [*Ferguson et al.*, 1993] to explore changes in the thermal regime and updip limit of seismicity with variations in dehydration reaction kinetics and trench parallel fluid pressure. On the EPR side of the plate suture, *Spinelli and Saffer* [2004] accounted for the presence of hydrothermal circulation and shut it off either at the trench or 10 km downdip. On the CNS side of the plate suture, *Spinelli and Saffer* [2004] assumed conductive heat flow. The models of *Spinelli and Saffer* [2004] are slightly warmer but generally agree with those of *Harris and Wang* [2002].

[18] North of our study area, *Heesemann et al.* [2009] estimated the temperature in the rupture area of the 1992 Nicaragua tsunami earthquake. Their thermal model is based on half-space cooling using parameters estimated by *Stein and Stein* [1992] with the exception of temperatures within the upper oceanic crust that were cooled to account for hydrothermal circulation. Similar to *Harris and Wang* [2002] they assumed hydrothermal circulation ceased when the plate entered the subduction zone.

[19] *Peacock et al.* [2005] developed a set of thermal models for the Costa Rica and Nicaragua segments of the subduction zone with a focus on slab dehydration reactions in the deeper part of the system. They recognized that regional heat flow values associated with EPR crust are low and consistent with vigorous hydrothermal circulation, but used conductive models to define the lithospheric geotherm of the incoming plate. They found only minor variations in the thermal structure of the deep portion of the subduction zone across the plate suture.

[20] We build on these previous models in two ways. We use a much larger set of heat flow data on the margin [*Harris et al.*, 2010] that was not available for these earlier studies. Second we incorporate more realistic simulations of fluid flow within the subducting aquifer and explore the alongstrike implications of hydrothermal circulation.

[21] In this study we construct two-dimensional finite element thermal models along 16 transects corresponding to seismic and heat flow profiles that cross the margin (Figure 1). For each transect a steady state thermal model is created using the algorithm developed and described by *Wang et al.* [1995]. This model solves the heat conduction – advection equation using a finite element approach. Heat is transferred advectively with the subducting plate and conductively through the fore arc. The thermal effects of mantle wedge flow are coupled to the subducting slab using an isoviscous mantle rheology [*Peacock and Wang*, 1999]. The details of the mantle rheology have only a small effect on the seismogenic portion of the subduction thrust [*Currie et al.*, 2002].

[22] The upper boundary for the model has a fixed temperature of 0°C, and the base of the subducting plate is assigned a temperature of 1400°C. The thermal regime of the subduction thrust is insensitive to this basal boundary condition. The landward boundary is also placed sufficiently far from the seismogenic zone to avoid boundary effects. At the landward boundary, we prescribe a surface heat flow of 70 mW m^{-2} and an adiabatic gradient through the mantle wedge. This heat flow is consistent with a back-arc setting.

Table 1. Model Parameters

Seismic Line	Plate Age (Ma)	Convergence Rate[a] (mm yr^{-1})	Azimuth (deg)
BGR99-41	24	87	32
BGR99-39	24	87	32
BGR99-43	24	87	33
BGR99-44	24	88	33
SO81-8	22	91	33
SO81-9	22	91	33
SO81-21	22	93	33
SO81-15	20	93	33
SO81-13	18	95	33
SO81-2	18	95	33
SO81-3	18	95	33
SO81-4	18	96	33
BGR99-17	17	96	33
SO81-5	17	96	33
BGR99-15	16	96	33
P-1600	16	96	33

[a]Convergence rates are given along azimuth of seismic line.

[23] Parameters strongly influencing the thermal regime of the subduction zone include: the initial geotherm of the incoming oceanic plate, the convergence rate, the geometry of subduction, and frictional heating along the plate interface [*Cloos*, 1985; *Dumitru*, 1991]. Reasonable variations in thermal physical rock properties have a lesser effect on the thermal regime. Each of these parameters is described and the sensitivity of the models to these parameters is explored in sections 4.1–4.3.

4.1. Model Geometry and Thermal Physical Rock Properties

[24] For each model transect the geometry of the oceanic plate is defined using seismic reflection and refraction data, Wadati-Benioff earthquakes, and tomographic images of the slab [*Ranero et al.*, 2005]. In the models the continental Moho is set to a depth of 40 km [*DeShon et al.*, 2006; *MacKenzie et al.*, 2008].

[25] The age and convergence rate associated with each transect are given in Table 1. Plate convergence rates are well established and only slightly oblique. We model the orthogonal component assuming the trench parallel component has little effect on the thermal regime. Offshore the northern Nicoya Peninsula, plate age is relatively well constrained at 24 Ma and isochrons are parallel to the trench. South of the plate suture magnetic isochrons intersect the trench with a high angle. Our thermal models are steady state and we explore variations in plate age with sensitivity tests to qualitatively indicate the impact of transient warming or cooling.

[26] Regionally extensive sills in EPR crust offshore the Nicoya Peninsula have been identified through drilling at ODP Site 1039 [*Kimura et al.*, 1997] and as a smooth high-amplitude seismic reflection [*Silver et al.*, 2004]. At ODP Site 1039 sediment immediately above the sills is dated at 16.5 Ma and the sills may be 13–14.5 Ma based on ages of dredged rocks from the Cocos and Fisher ridges [*Werner et al.*, 1999]. Emplacement of these sills may thermally rejuvenate the plate, but the effect is small and short lived; in general, sills cool relatively quickly [*Jaeger*, 1964]. The thermal effect of a infinite 200 m thick sheet buried beneath 400 m of sediments [*Kimura et al.*, 1997] and having an initial temperature contrast of 1000°C decays to less than 5 mW m^{-2} in 0.3 Myr.

[27] Geometrically, each model consists of five units: the oceanic plate, sediments, margin, the Chorotega block, and mantle wedge (Figure 3). Because the Chorotega block has an oceanic affinity and also forms the crystalline portion of the margin these units are given the same thermal parameters as the oceanic plate (Table 2). Parameter values are consistent with those used in other modeling studies for the oceanic plate [e.g., *Hyndman and Wang*, 1993; *Oleskevich et al.*, 1999; *Currie et al.*, 2002] but larger than those used by *Heesemann et al.* [2009]. The mantle wedge is assigned a thermal conductivity of 3.1 W m^{-1} K^{-1} and the heat capacity of the oceanic plate and mantle wedge is 3.3 MJ m^{-3} K^{-1}.

[28] At the MAT the ~375 m of sediment consists of hemipelagic and pelagic sediments. Offshore of the Nicoya Peninsula sediment thickness is relatively uniform except where seamounts and basement highs decrease sediment thickness [*Spinelli et al.*, 2006]. Sediment thickness to the south is more variable where basement highs disrupt sedimentation patterns. A uniform sediment thickness of 350 m is used for all models. Modest variations in sediment thickness do not appear to influence our interpretations. The oceanic sediments have a thermal conductivity of 0.9 W m^{-1} K^{-1}, a radioactive heat production of 0.2 μW m^{-3} and a heat capacity of 2.6 MJ m^{-3} K^{-1}.

4.2. Initial Geotherm and Hydrothermal Circulation

[29] The thermal state of the oceanic crust entering the subduction system exerts a fundamental influence on subduction zone temperatures [e.g., *Dumitru*, 1991]. Because of strong along-strike variations in the observed heat flow of the incoming plate

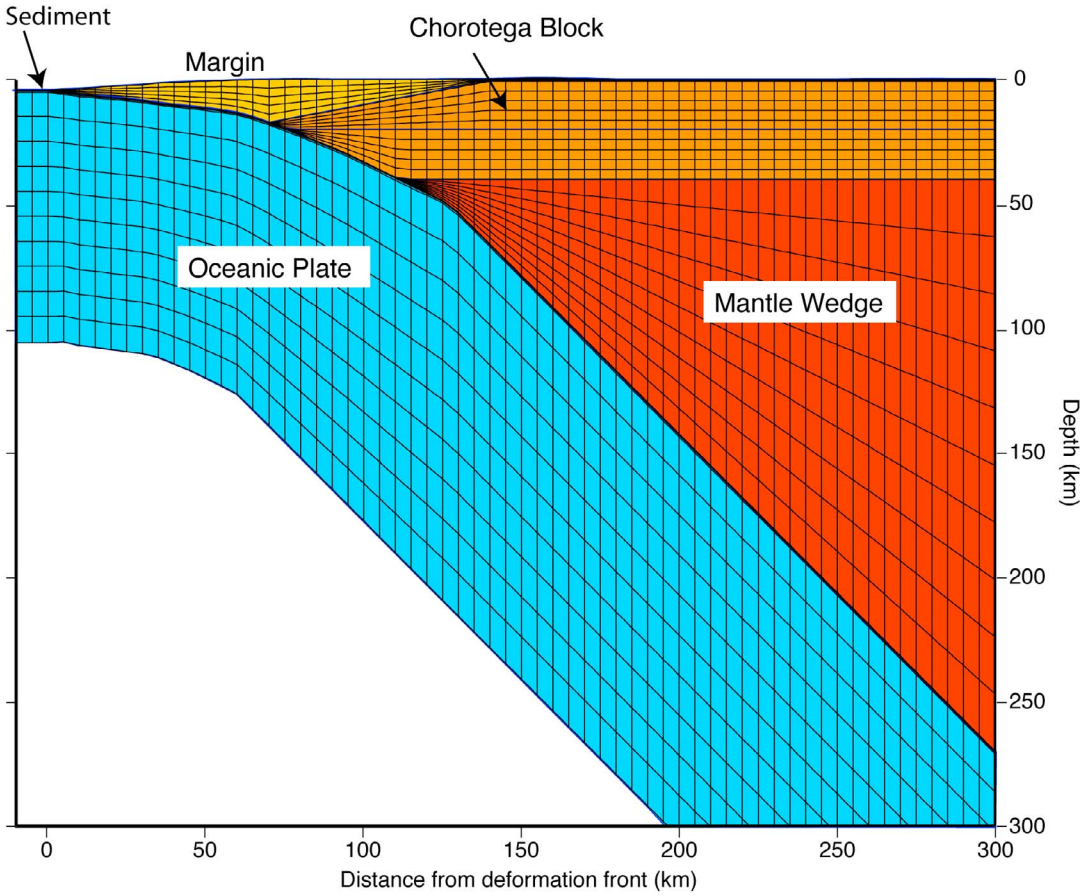

Figure 3. Representative mesh and units of subduction zone model. A 350 m layer of sediments sits on top of the oceanic plate. The upper 500 m of the oceanic plate forms the aquifer. Both the margin and crust form the Chorotega block.

[e.g., *Fisher et al.*, 2003; *Hutnak et al.*, 2007] and the discrepancy in these values from age-dependent conductive predictions, we focus on the initial geotherm. We use a one-dimensional geotherm to define the thermal structure of the incoming oceanic plate and explore the sensitivity of our models to thermal states that corresponds to conductive and advective fluid flow regimes within the upper oceanic crust. For each transect, the first set of modeled geotherms (Figure 4) assumes conductive half-space cooling based on the age of the crust at the trench (Table 1). The change in gradient associated with the sediment layer is due to the change in thermal conductivity. Scenarios with this geotherm are the warmest of the three scenarios explored and are termed "conductive" models. Models initialized with this geotherm do not incorporate fluid flow.

[30] Because of the evidence for hydrothermal circulation in the incoming oceanic crust (Figure 2) [*Fisher et al.*, 2003; *Hutnak et al.*, 2007], and because many of the heat flow profiles on the margin appear to not conform with conductive predictions [*Harris et al.*, 2010], we investigate the role regional hydrothermal circulation has on influencing temperature along the subduction thrust. The remaining two geotherms are associated with an isothermal aquifer 500 m thick and half-space cooling below the aquifer (Figure 4). A 500 m thick aquifer is consistent with previous studies offshore the Nicoya Peninsula [*Harris and Wang*, 2002; *Fisher et al.*,

Table 2. Model Parameters

Unit	Thermal Conductivity ($W\ m^{-1}\ K^{-1}$)	Heat Capacity ($MJ\ K^{-1}\ m^{-3}$)	Heat Production ($\mu W\ m^{-3}$)
Chorotega block (0–40 km)	2.9	–	0.2
Margin	2.9	–	0.2
Sediments (0.4 km)	0.9	2.6	0.2
Oceanic plate	2.9	3.3	0.3
Mantle wedge	3.1	3.3	0.2

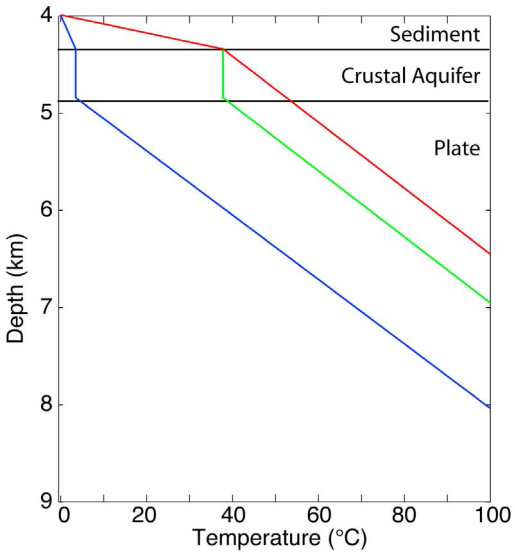

Figure 4. Geotherms defining the initial thermal state of the subducting oceanic crust. The conductive geotherm (red) corresponds to conductive half-space cooling model appropriate for the age of the crust (Table 1). The change in gradient through the sediments is due to the contrast in thermal conductivity between the sediments and oceanic crust. The intermediate geotherm (green) has the same gradient through the sediments as the conductive geotherm but includes an isothermal aquifer of 0.5 km. This geotherm is coupled with insulated circulation models and of the hydrothermal circulations model explored corresponds to minimal heat loss. The cold geotherm (blue) is parameterized with a fixed gradient (10°C/km) through sediments and an isothermal aquifer. This geotherm is used to initialize the ventilated and conductive rebound simulations and corresponds to large heat extraction.

2003; *Spinelli and Saffer*, 2004; *Hutnak et al.*, 2007] and other studies of fluid flow in oceanic crust [e.g., *Davis et al.*, 1997]. For these geotherms, the aquifer temperature is equal to the temperature at the base of the sediments.

[31] Our intermediate geotherm uses a thermal gradient through the sediments based on conductive cooling. This intermediate geotherm is appropriate for hydrothermal circulation within an aquifer insulated by sediments. In these insulated models heat is brought up from depth along the subducted aquifer and carried laterally along the seaward continuation of the aquifer. Conceptually, this scenario corresponds to low-permeability sediment isolating fluid flow within crustal aquifer. Models initialized with this geotherm and having this flow pattern are termed "insulated." These models are used to characterize the heat flow observations south of the plate suture [*Harris et al.*, 2010].

[32] The third geotherm consists of an imposed low thermal gradient through the sediments corresponding to an observed heat flow of 10 mW m^{-2} (Figure 4). The low thermal gradient is appropriate for hydrothermal circulation associated with cool well-ventilated crust where fluids freely communicate with the overlying ocean at the trench axis. This scenario is the coolest of the three scenarios investigated in this study. Models initialized with this geotherm and having this style of flow are termed "ventilated" models. These models are used to characterize heat flow observations north of the plate suture.

[33] We incorporate the effects of hydrothermal circulation within the aquifer using a Nusselt number approach [*Spinelli and Wang*, 2008; *Kummer and Spinelli*, 2008, 2009]. The Nusselt number approximation has been successfully applied to systems where vigorous circulation efficiently transports heat [*Davis et al.*, 1997]. The Nusselt number, *Nu*, is the ratio of heat transport to heat that would be transferred by conduction alone,

$$Nu = \frac{q}{\lambda \Gamma}, \tag{1}$$

where q is the total heat transport, λ is the thermal conductivity, and Γ is the thermal gradient. This approach is implemented by increasing the thermal conductivity within the model aquifer. *Nu* is specified in a multistep procedure [*Spinelli and Wang*, 2008] whereby conductive simulations are used to initialize heat flux into the base of the aquifer and temperature-dependent values of fluid density, ρ_f, viscosity, μ, thermal expansivity, α, and thermal diffusivity, κ, are computed throughout the aquifer using a look-up table for appropriate temperatures and pressures [*Harvey et al.*, 1997]. These values are used to compute the Rayleigh number, *Ra*, for a prescribed depth-dependent permeability, k,

$$Ra = \frac{\alpha g k L^2 \rho_f q}{\lambda \mu \kappa} \tag{2}$$

where g is the acceleration of gravity, and L is aquifer thickness. Following *Spinelli and Wang* [2009], we specify permeability through the equation,

$$\log(k) = -9 - 5.5 \times 10^{-5}(z - 600) \tag{3}$$

where z is the depth below the seafloor in meters. *Spinelli and Wang* [2009] found this gradual decrease in permeability with depth yields modeled surface heat flux consistent with observations for the Nankai subduction zone. Our results suggest

that once the permeability decreases to values less than 10^{-12} m^2, the thermal structure is only slightly different from conductive models. This depth corresponds to approximately 20 km and is the deepest depth for which the modeled upper oceanic crustal aquifer simulates the transfer of heat by fluid flow. For regions shallower than this depth heat is transferred up along the aquifer and warms the trench. *Nu* is estimated through a scaling relationship

$$Nu = 0.08Ra^{0.89}, \quad (4)$$

determined by comparing results using the conductive proxy for fluid flow to those from simulations with coupled heat and fluid flow for the same problem [*Kummer and Spinelli*, 2008]. Once *Nu* is determined, an effective thermal conductivity is calculated and new temperatures are computed. This procedure is repeated until the temperatures stabilize.

[34] Finally, we investigate the impact of allowing the cold geotherm to conductively rebound once the plate enters the subduction zone. This scenario corresponds to hydrothermal circulation shutting off at the trench and is consistent with the modeling approach of *Harris and Wang* [2002] as suggested by *Langseth and Silver* [1996]. These "conductive rebound" models are only explored for heat profiles north of the plate suture.

4.3. Frictional Heating

[35] The thermal structure of the subduction thrust is sensitive to frictional heating [e.g., *van den Beukel and Wortel*, 1988; *Molnar and England*, 1995; *Dumitru*, 1991]. *Hyndman* [2007] reviews evidence supporting low values of effective coefficients of friction on subduction thrusts. Both thermal and geomechanical data have been interpreted to suggest a low value for this parameter [*Wang et al.*, 1995]. Additionally, tectonically eroding margins may have lower effective coefficient values of friction than accreting margins. The transfer of material from the overriding plate to the underthrusting plate characterizes tectonically erosive margins as the subduction thrust migrates upward [*von Huene et al.*, 2009]. This migration has been hypothesized to occur through hydrofracturing of rocks by over pressured fluids that inject from the interplate boundary into the base of the overriding plate [*von Huene and Ranero*, 2003; *Sage et al.*, 2006; *Calahorrano et al.*, 2008; *Ranero et al.*, 2008]. Overpressures decrease the coefficient of effective friction.

[36] Although our reference models do not incorporate frictional heating, we explore its effect following the methods implemented by *Wang et al.* [1995]. We consider two segments along the plate interface, an upper segment of frictional sliding, and a lower segment of ductile shear [*Wang et al.*, 1995; *Currie et al.*, 2002]. Along the upper frictional sliding segment, the shear stress is specified by Byerlee's law [*Byerlee*, 1978] and increases with depth due to the increasing normal stress from the load of the overlying material. The pore pressure ratio defined as the ratio of pore pressure to lithostatic stress is assumed to be constant with depth, 0.85, and the effective coefficient of friction is assumed to be 0.03. Below the brittle sliding regime the magnitude of heating per unit volume is given by the product of the shear stress and strain rate along the fault to a depth of 40 km where the overriding Moho intersects the subduction thrust. The viscous stress is determined from the strain rate using the power law rheology for diabase [e.g., *Caristan*, 1982]. The magnitude of shear stress decreases with depth as temperature increases. Below the Moho the interface between the down going plate and the serpentinized mantle wedge is believed too weak to generate significant heating [e.g., *Currie et al.*, 2002].

5. Sensitivity Tests

[37] Thermal models of subduction are known to be relatively sensitive to plate age, convergence rate, frictional heating and subduction geometry [*Dumitru*, 1991; *Hyndman and Wang*, 1993; *Hippchen and Hyndman*, 2008; *Heesemann et al.*, 2009]. The age of the plate is used to establish the initial conductive geotherm and heat content of the subducting plate. The convergence rate and geometry govern the advection of heat by the down going slab and frictional heating is effectively a source term along the plate interface. In contrast to these parameters, these thermal models are less sensitive to reasonable variations in the thermal physical rock properties, including the fore-arc thermal conductivity and radiogenic heating [*Dumitru*, 1991; *Hyndman and Wang*, 1993; *Hippchen and Hyndman*, 2008; *Heesemann et al.*, 2009]. We characterize the sensitivity of isotherms to model parameters by investigating the sensitivity of the intersection of the 100°, 150°, and 350°C isotherms with the subduction thrust.

[38] We investigate models along two heat flow transects, one representative of conductive or insulated hydrothermal circulation south of the

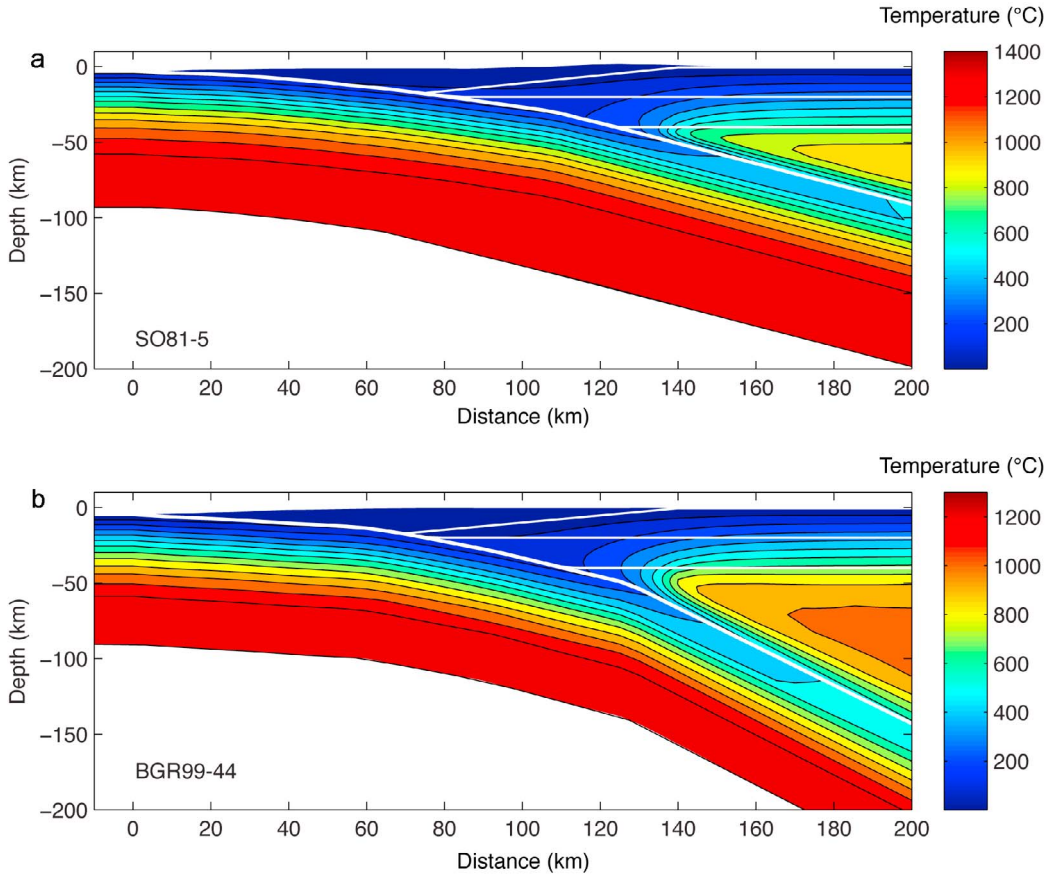

Figure 5. Thermal models for transects (a) SO81-5 south of the plate suture and (b) BGR99-44 north of the plate suture. Transect SO81-5 is initialized with the intermediate geotherm and models insulated hydrothermal circulation. Transect BGR99-44 is initialized with the cold geotherm and models ventilated hydrothermal circulation. The impact of these choices is most clearly observed on isotherms intersecting the shallow subduction thrust. Deeper in these models differences in the thermal regime are due to differences in their ages, convergence rates (Table 1), and geometry.

plate suture (SO81-5) and the other representative of ventilated circulation or conductive rebound north of the plate suture (BGR99-44) (Figure 1). Reference models for transects SO81-5 and BGR99-44 are portrayed in Figure 5. Transect SO81-5 is initialized with the intermediate geotherm and circulation is insulated. Transect BGR99-44 is initialized with the cold geotherm and circulation is ventilated. Transect SO81-5 shows the shallower dip appropriate south of the plate suture. Temperatures along the shallow subduction thrust are warmer along transect SO81-15 than BGR99-44 because of the warmer initial geotherm and insulated circulation.

[39] Heat flow profile SO81-5 is used to explore the influence of model parameters and conductive versus insulated circulation on the position of the selected isotherms. Figure 6a shows the position of these isotherms on the subduction thrust as a function of the model parameter being explored. The first set of tests labeled "Initial Geotherms" investigates variations in the thermal regime between the conductive cooling and insulated hydrothermal circulation models. The intersection of the 350°C isotherm with the subduction thrust is below the area of high permeability and is relatively insensitive to the differences between the conductive and insulated flow models. In the region of the 150° and 100°C isotherm, where aquifer permeability is sufficient for fluid flow, heat is advected toward the trench lowering temperatures relative to the conductive model. Near and seaward of the trench temperatures are increased relative to the conductive model. These general results are consistent with the findings of *Kummer and Spinelli* [2008]. In the remainder of Figure 6a we vary plate age, convergence velocity,

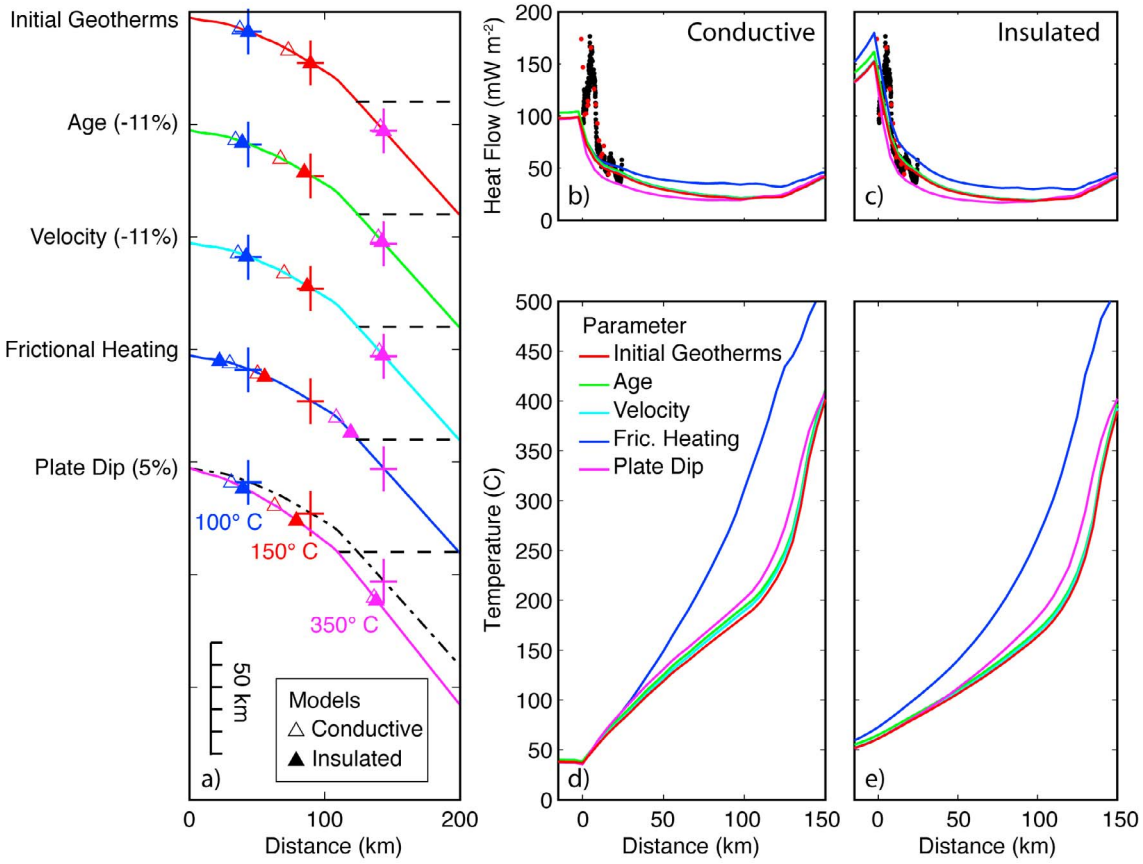

Figure 6. Sensitivity tests for profile SO81-5 south of the plate suture. (a) Influence of selected parameter on thermal state of the subduction thrust. The left-hand labels give the parameter being varied, and the percentage gives the magnitude of variation relative to values in Table 1. For example, plate age refers to decreasing the age of the plate from 17 to 15 Ma (11%), frictional heating is implemented as described in the text, and plate dip refers to uniformly increasing the plate dip by 5% relative to the reference plate dip (dash-dotted line). Colored lines show the subduction thrust and are color coded by the parameter being varied. These colors are used consistently throughout Figure 6. Open triangles correspond to conductive models, and solid triangles correspond to insulated circulation models. The blue, red, and magenta symbols correspond to the positions of the intersections of the 100°C, 150°C, and 350°C isotherms with the subduction thrust. Horizontal dashed line corresponds to the continental Moho. The cross along each profile corresponds to the position of the isotherms in the reference model and the leg of each cross corresponds to 20 km. The sensitivity of surface heat flow to variations in these parameters for (b) conductive and (c) insulated circulation patterns. Red and black circles show heat flow values based on seafloor probes and bottom-simulating reflectors, respectively [*Harris et al.*, 2010]. (d and e) The sensitivity of subduction thrust temperatures to variations in these parameters. Lines are color coded by the parameter being varied.

frictional heating and plate dip and plot the position of the selected isotherms as a function of model being tested, either the conductive or insulated model. The percentage variations for plate age and convergence rate are relative to values in Table 1. Frictional heating is implemented as described above and plate dip is uniformly increased by 5%. These tests show that the position of temperatures along the subduction thrust is very sensitive to frictional heating [e.g., *Dumitru*, 1991] followed in importance by the initial geotherm and presence of hydrothermal circulation and then plate dip for the given variations.

[40] An alternative view of these results is shown in Figures 6d and 6e where temperatures along the plate interface are plotted as a function of distance from the trench. With the exception of frictional heating and to a lesser extent plate dip, the temperature structure of the subduction thrust is relatively similar across these parameter variations. Note that temperatures for the insulated circulation simulations are more tightly grouped than the conductive

simulations indicating the homogenizing effect of fluid flow. Also notable when comparing Figures 6d and 6e, is that temperatures along the subduction thrust between approximately 30 and 100 km for the insulated model are lower than the conductive model. This relationship changes within about 20 km of the trench where the insulated models generate warmer temperatures along the subduction thrust.

[41] Figures 6b and 6c show the sensitivity of surface heat flow to conductive and insulated circulation, respectively. Near the trench, heat flow profiles are much more sensitive to the presence or absence of insulated circulation than to reasonable variations in model parameters. Models incorporating the Nusselt number approximation for insulated circulation fluid flow fit the heat flow data along profile SO81-5 much better than purely conductive models. Together, the plots in Figure 6 show the issue of nonuniqueness associated with thermal models of subduction zones and show that although temperature on the subduction thrust is very sensitive to frictional heating, surface observations of heat flow are much less sensitive to this parameter and are more sensitive to the initial geotherm and presence of hydrothermal circulation.

[42] To evaluate the sensitivity of model parameters to ventilated circulation scenarios that may be characteristic of the thermal regime north of the plate suture we use profile BGR99-44 (Figure 7). We investigate three sets of simulations corresponding to (1) the conductive model, (2) the conductive rebound in which the cold geotherm (Figure 4) is allowed to relax once the plate enters the subduction zone [*Harris and Wang*, 2002], and (3) the ventilated model initialized with the cold geotherm and for which circulation continues as the plate subducts. Models initialized with the cold geotherm contain much less heat than those initialized with the conductive and intermediate geotherms. The intersection of the 100° and 150°C isotherms with the subduction thrust for these models is always deeper than for conductive models (Figure 7a). Even though the ventilated and conductive rebound models are initialized with the same geotherm, the ventilated models are cooler in this region because ventilated circulation keeps the subduction thrust cool. The heat advected from depth does not warm the trench because this heat is immediately vented to the ocean. By about 100 km from the trench, corresponding to the intersection of the subduction thrust with the Moho and below the depth where permeability allows vigorous circulation, temperatures along the subduction thrust are similar (Figures 7d and 7e). As with the insulated models, incorporating frictional heating into the models has the biggest impact on subduction thrust temperatures.

[43] The sensitivity of surface heat flow to these models is shown in Figures 7b and 7c. Although not directly compared in Figure 7, heat flow profiles and subduction thrust temperatures are only slightly cooler for ventilated models than the conductive rebound model. On the basis of the heat flow data it is not possible to discriminate between these models. For the simulations considered here, frictional heating on the subduction thrust is the largest uncertainty and the temperatures on the subduction thrust are more sensitive to this effect than surface observations of heat flow (Figures 6 and 7). In the results that follow we do not include frictional heating and the estimated position of our isotherms represents a maximum depth for each simulation.

6. Results

[44] Results from the various simulations, arranged from north to south, are compared to the heat flow data (Figure 8). We view models as a function of initial geotherm and the presence or absence of hydrothermal circulation. Our intent is to fit the low wave number variation in the data at a reasonable level with a consistent set of model parameters. For each transect we show the conductively cooling model and insulated circulation simulations initialized with the intermediate geotherm. These two sets of simulations show relatively high heat flow at the trench that decreases landward consistent with heat being advected downward by the subducting slab. In addition, for transects north of the plate suture where heat flow is relatively low, we also show simulations initialized with the cold geotherm for ventilated circulation and conductive rebound. As in the sensitivity simulations (Figure 7) these models generate only a small difference in surface heat flow such that it is not possible to discriminate between these two scenarios using the heat flow data alone. Our preferred model for each transect is given in Table 3.

[45] Of the four heat flow transects associated with EPR crust, transect BGR99-44 is the best characterized. Heat flow data along this transect are most consistent with the cold initial geotherm. Although differences in the surface heat flow due to continuing or stopping circulation upon subduction are small, this difference has important implications for

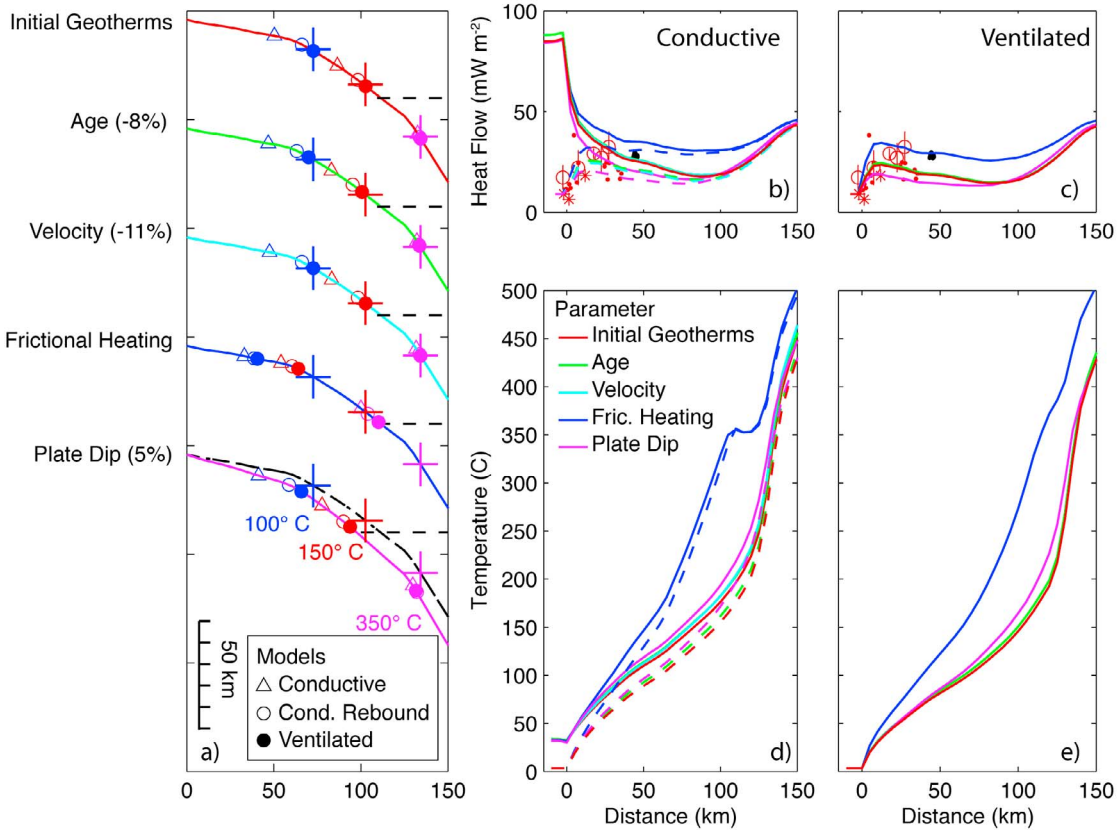

Figure 7. Sensitivity tests for profile BGR99-44 north of the plate suture. (a) Influence of selected parameter on thermal state of the subduction thrust. The left-hand labels give the parameter being varied, and the percentage gives the magnitude of variation relative to values in Table 1. For example, plate age refers to decreasing the age of the plate from 24 to 22 Ma (8%), frictional heating is implemented as described in the text, and plate dip refers to uniformly increasing the plate dip by 5% relative to the reference plate dip (dash-dotted line). Colored lines show the subduction thrust and are color coded by the parameter being varied. Open triangles correspond to conductive models, and solid triangles correspond to insulated circulation models. The blue, red, and magenta symbols correspond to the positions of the intersections of the 100°C, 150°C, and 350°C isotherms with the subduction thrust. Horizontal dashed line corresponds to the continental Moho. The cross along each profile corresponds to the position of the isotherms in the reference model and the leg of each cross corresponds to 20 km. The sensitivity of surface heat flow to variations in these parameters for (b) conductive and (c) ventilated circulation patterns. Dashed lines in Figure 7b correspond to conductive rebound model. Red and black circles show heat flow values based on probes and bottom-simulating reflectors, respectively [*Harris et al.*, 2010]. Open circles correspond to heat flow data of *Langseth and Silver* [1996] averaged over 5 km, and stars correspond to ODP heat flow values [*Ruppel and Kinoshita*, 2000]. (d and e) The sensitivity of subduction thrust temperatures to variations in these parameters. Lines are color coded by the parameter being varied.

our understanding of the flow system and temperatures along the subduction thrust. Choosing the appropriate thermal model for profiles north of BGR99-44 is less straightforward. Heat flow derived from BSRs along transect BGR99-39 and BGR99-41 do not get close enough to the trench to discriminate between the models. Both of these transects show BSRs disappearing into the margin basement and we infer that if the subduction interface warmed near the trench consistent with the conductive geotherm BSRs would be visible to the deformation front. Additional evidence for favoring the cold initial geotherm includes the low regional heat flow seaward of the trench (Figure 2) and because thermal modeling of the subduction zone offshore Nicaragua suggests that the cool region continues to the north [*Heesemann et al.*, 2009]. It does appear however, that these profiles are slightly warmer than BGR99-44. Along transect BGR99-39 there are three high heat flow measurements approximately 15 km from the trench axis that appear to match the intermediate

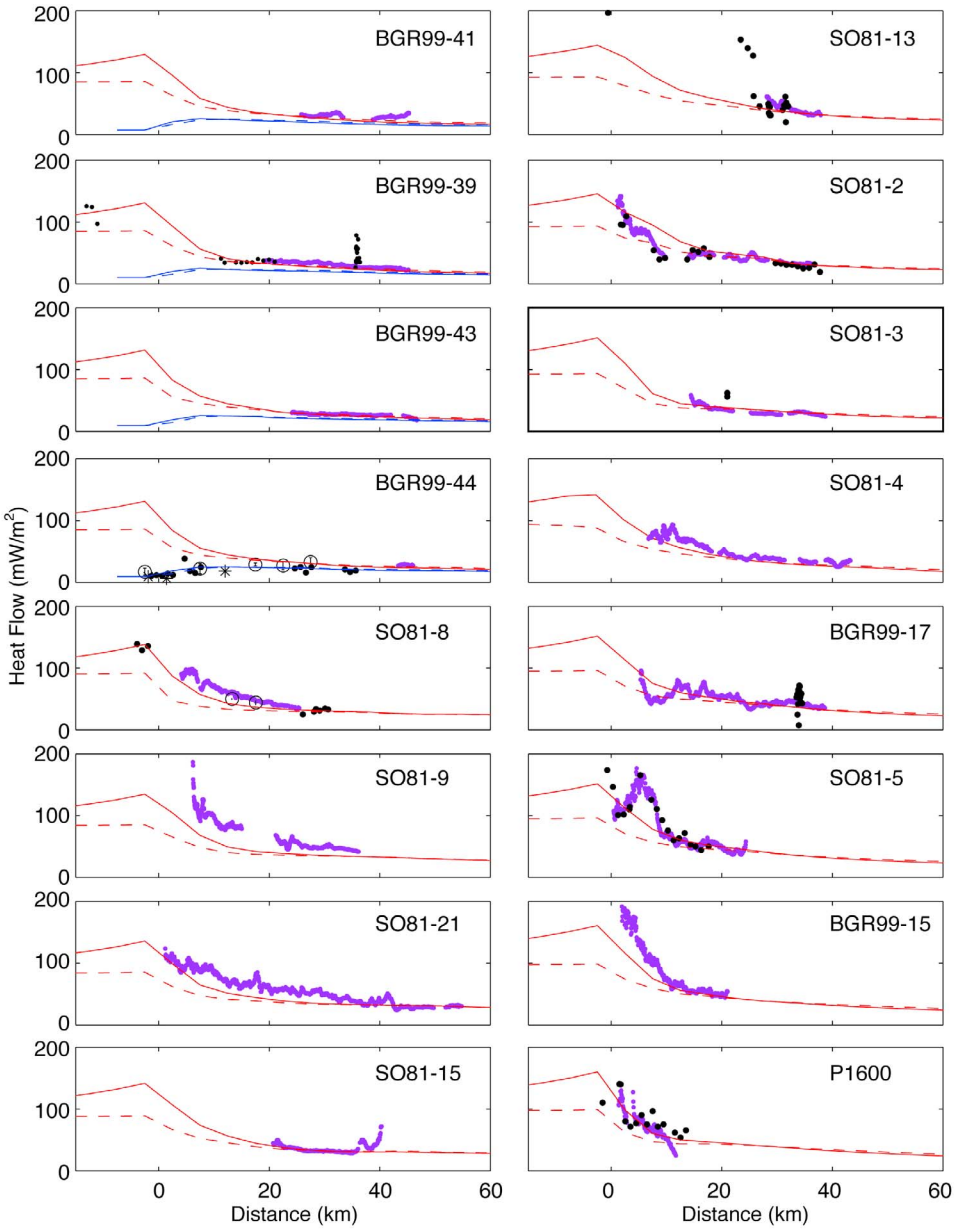

Figure 8. Comparison of heat flow data and simulations. Black solid circles show seafloor probe observations of heat flow, and purple circles show heat flow derived from bottom-simulating reflectors [*Harris et al.*, 2010]. The red dashed line corresponds to conductive predictions, and the red solid line corresponds to the intermediate geotherm (Figure 4) and insulated circulation. North of the plate suture where heat flow values are low we investigate models corresponding to the coldest initial geotherm with ventilated circulations (solid line) and conductive rebound (dashed line). Open black circles along profiles BGR99-44 and SO81-8 are heat flow data of *Langseth and Silver* [1996] averaged in 5 km windows, and stars are heat flow values from Leg 170 [*Ruppel and Kinoshita*, 2000].

geotherm with insulated circulation. However, this feature suggests to us local fluid discharge [*Hutnak et al.*, 2007]. For consistency with transect BGR99-44, we prefer the model with a cold initial geotherm and ventilated circulation for transects north of the plate suture (Table 3) but acknowledge that our preferred models are not required by the heat flow data. These transects show the importance of obtaining heat flow values seaward and within 5–10 km of the trench axis to discriminate between warm and cold initial geotherms.

[46] South of the plate suture, heat flow values near the trench are considerably higher and for the most

Table 3. Preferred Models

Seismic Line	Initial Geotherm[a]	Circulation Style[b]
BGR99-41	Cold	Ventilated
BGR99-39	Cold	Ventilated
BGR99-43	Cold	Ventilated
BGR99-44	Cold	Ventilated
SO81-8	Intermediate	Insulated
SO81-9	Intermediate	Insulated
SO81-21	Intermediate	Insulated
SO81-15	Intermediate	Insulated
SO81-13	Intermediate	Insulated
SO81-2	Intermediate	Insulated
SO81-3	Intermediate	Insulated
SO81-4	Intermediate	Insulated
BGR99-17	Intermediate	Insulated
SO81-5	Intermediate	Insulated
BGR99-15	Intermediate	Insulated
P-1600	Intermediate	Insulated

[a]Initial geotherms are depicted in Figure 4.
[b]Ventilated refers to models where hydrothermally advected heat is extracted at the trench and insulated refers to models where hydrothermally advected heat is transported laterally and seaward of the trench within the crustal aquifer.

part appear consistent with the intermediate geotherm and insulated circulation simulations. These features include the high heat flow near the trench that decline landward (SO81-8, SO81-9, SO81-21, SO81-2, SO81-5, BGR99-15, and P1600). However, transects SO81-15 through SO81-3 (generally within the seamount segment) appear relatively disrupted, and heat flow values are generally well landward of the trench making discrimination between these sets of simulations less conclusive.

[47] Figure 9 shows temperature along the top of the subducting plate for our preferred models. The transition from the cold EPR crust north of the plate suture to the warmer CNS south of the plate suture is displayed most dramatically by the 100°C isotherm. Along the northern Nicoya Peninsula the 100°C isotherm is just offshore but then abruptly moves seaward near the plate suture and remains closer to the trench axis to the south. This bend is present to some extent in all of the plotted

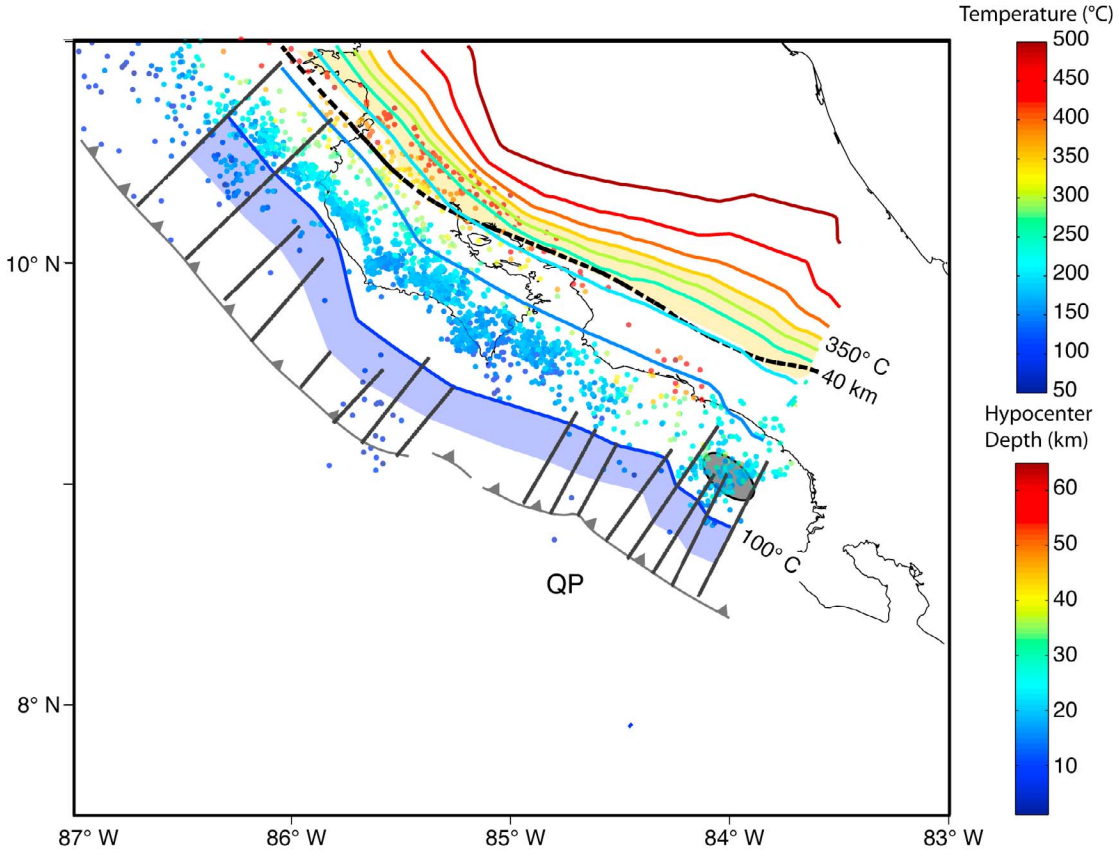

Figure 9. Plate interface isotherms corresponding to preferred thermal models (Table 3). Grey lines show positions of thermal models. The contour interval is 50°C. The blue shaded and orange shaded regions show the seaward displacement of isotherm corresponding to modest frictional heating. The intersection of the Moho with the subduction thrust is shown by bold dashed line [*Ranero et al.*, 2005]. Hypocenters are from *Ghosh et al.* [2008]. The shaded region is the rupture area for the 20 August 1999 M_w 6.9 event downdip of the Quepos Plateau (QP) [*Bilek*, 2007].

isotherms, but decreases landward as the influence of the initial condition decreases. In reality, this transition is likely to attenuate with depth due to along-margin diffusion of heat not accounted for in these two-dimensional models. The region associated with EPR crust north of the plate suture shows the largest change relative to conductive predictions, consistent with the sensitivity analysis. South of the plate suture the warmer isotherms spread out as a result of the of the decreasing subduction dip. The depth to the 40 km contour along the subduction slab (dashed line) shows the intersection of the continental Moho with the subducting plate interface. This level roughly tracks with the 200°C isotherm. The 350°C isotherm falls within the mantle wedge in all locations.

[48] These isotherms represent a maximum depth because we have not included the effects of frictional heating along the plate interface. Most subduction thrust faults are believed to be frictionally weak and thus have low frictional heat production [*Dahlen et al.*, 1984; *Byrne and Fisher*, 1990; *Wang et al.*, 1995; *Wang and He*, 1999]. However, a sense for the potential magnitude of this effect is given in the sensitivity analysis. For transect SO81-5, representative of CNS crust, the 100°, 200° and 300°C isotherms move seaward 20, 40, and 30 km, respectively (Figure 6e). For transect BGR99-44, representative of EPR crust, the 100°C, 200°C, and 350°C isotherms move seaward approximately 30, 40, and 30 km, respectively (Figure 7e). Shaded bands (Figure 9) show the seaward translation of the 100°C and 350°C isotherm due to the effects of frictional heating. With frictional heating the 350°C isotherm roughly corresponds to the intersection of the continental Moho with the subduction thrust.

7. Discussion

[49] Our results point to the significance of the change in thermal regime between EPR and CNS crust in modulating the thermal structure of the shallow subduction thrust. Heat flow data seaward of the trench clearly indicates that the thermal transition is due to fluid flow in the oceanic crust [*Fisher et al.*, 2003; *Hutnak et al.*, 2007]. Processes controlling this thermal transition are not well understood. *Fisher et al.* [2003] considered a number of hypotheses and favored two. The first hypothesis is that the lateral permeability of EPR crust may be significantly greater than CNS crust. Enhanced lateral permeability coupled with seamounts that penetrate otherwise continuous sediment cover would increase the removal of heat through lateral fluid flow [*Hutnak et al.*, 2007, 2008]. They also speculated that intrusions and high-angle faulting of basement rocks during the construction of CNS crust might lead to hydrogeologic compartmentalization. Both conditions would facilitate removing large quantities of heat within EPR crust while suppressing advective heat removal within CNS crust. Our choice of a cold geotherm and ventilated circulation in EPR crust is consistent with these hypotheses. Unfortunately, heat flow measurements on the margin do not discriminate between ventilated hydrothermal circulations models from the conductive rebound models. We posit that continuing hydrothermal circulation in the down going plate is likely if plate bending normal faults observed in the trench are not barriers to fluid flow. In general fault offsets are less than 500 m [*Ranero et al.*, 2003], the modeled depth of the regional upper oceanic crustal aquifer, and thus fault offsets would not prevent flow. However, if the plate bending faults lead to enhanced alteration that decreases permeability, the faults could constitute flow barriers resulting in a compartmentalized crustal aquifer. In this scenario the thermal regime might be best characterized by a cold geotherm that conductively relaxes once the crust enters the subduction zone. More detailed and fully coupled heat and fluid flow models associated with the plate bending normal faults might help resolve this issue.

[50] On CNS crust immediately south of the plate suture there is a conspicuous absence of outcrops [*Fisher et al.*, 2003]. Thermal models and regional heat flow data are consistent with an intermediate geotherm and insulated circulation that continues as the aquifer is subducted. Farther south through the seamount and Cocos Ridge segments exposed basement is common. Fluid flow between the incoming oceanic crust and the overlying ocean is likely occurring but does not appear to be extracting large quantities of heat as indicated by the large standard deviation and high mean of the regional heat flow data, respectively (Figure 2). In this region magnetic lineations enter the trench at a high angle (Figure 1) and active plate bending normal faults are not as prominent as they are north of the plate suture [*Ranero et al.*, 2005]. Studies of permeability anisotropy on the Juan de Fuca ridge flank indicate that permeability is higher parallel to ridge strike than perpendicular to it [*Fisher et al.*, 2008]. This permeability anisotropy may enhance downdip hydrothermal circulation within the plate producing a thermal structure consistent with simulations representing CNS crust.

[51] The influence of hydrothermal circulation and style of flow modeled here leads to generally cooler models and a cooler subduction thrust than earlier models suggested [*Harris and Wang*, 2002; *Spinelli and Saffer*, 2004]. These cooler temperatures primarily reflect the influence of hydrothermal circulation to greater depth than the previous models. These models are also cooler than models shown by *Ranero et al.* [2008], but those isotherms are based on simple downward extrapolation of temperatures from heat flux measurements, and do not take the advection caused by the plate convergence.

[52] Because temperature is thought to be a primary influence on the location of the seismogenic zone, it is interesting to compare the position of these new isotherms with microseismicity along the plate interface (Figure 9). Microseismicity along the plate interface come from events recorded by the CRSEIZE experiment. Details of the seismic portion of the CRSEIZE experiment, data processing, resolution, and interpretation are reported in a number of studies [*Newman et al.*, 2002; *DeShon et al.*, 2003, 2006; *Ghosh et al.*, 2008]. Event locations and a three-dimensional velocity structure were estimated through a simultaneous inversion of both P and S wave arrivals [*DeShon et al.*, 2003, 2006]. Shallow event locations are estimated to be better than 1 km in both horizontal and vertical directions. The plate interface is defined through the seismic velocity model and events within 5 km of this interface are assumed to be interplate earthquakes. Hypocenters down to approximately 30 to 40 km are on the plate interface [*DeShon et al.*, 2006], but deeper hypocenters between approximately 40 and 50 km may be either on the plate interface or within the subducting plate. Deeper events are within the plate.

[53] The cooler models presented here show that the 100°C isotherm is slightly updip of the dense trend in microseismicity offshore the northern Nicoya Peninsula on the EPR side of the plate suture. Northwest of the Nicoya Peninsula microseismicity extends farther seaward. This microseismicity near transects BGR99-39 and BGR99-41 may be associated with the 1992 Nicaragua tsunami event that ruptured through the updip limit of the seismogenic zone [*Satake*, 1994]. Alternatively, these profiles may be much warmer than suggested by the preferred thermal models using the cold initial geotherm. This interpretation however, is not supported by the regional heat flow data (Figure 2). Southeast of this region, the 100°C isotherm parallels the trench and the updip extent of microseismicity associated with the 1999 M_w = 6.9 Quepos earthquake [*DeShon et al.*, 2003]. The close correlation between the 100°C isotherm and changes in the updip extent of microseismicity is consistent with hypotheses that suggest the updip extent of the seismogenic zone has a thermal control [*Vrolijk*, 1990; *Hyndman and Wang*, 1993; *Oleskevich et al.*, 1999].

[54] Colored bands associated with the 100° and 350°C isotherms in Figure 9 show how modest frictional heating might warm the subduction thrust. Both bands are approximately 20 km wide. Modest frictional heating moves the 100°C isotherm to include some of the sparse seismicity north of the Nicoya Peninsula and moves the 350°C isotherm to a depth of approximately 40 km.

[55] Northwest of the Osa Peninsula, the M_w = 6.9 underthrusting earthquake appears to be influenced by subducting topography [*Bilek et al.*, 2003]. The along-strike rupture width corresponds to the width of the subducting Quepos Plateau. Aftershocks were captured by the CRSEIZE experiment [*DeShon et al.*, 2003] and a later portion of these aftershocks appear as two streaks correlated with basement highs on the Quepos Plateau [*Bilek et al.*, 2003; *DeShon et al.*, 2003]. The correlation between bathymetry highs and aftershocks led *DeShon et al.* [2003] to conclude that the aftershocks may not be rupturing the entire updip width of the seismogenic zone and they suggest that the updip limit may change through the seismic cycle. However, our thermal models capture the majority of microseismicity within the 100°C isotherm.

[56] The downdip extent of microseismicity is relatively diffuse and hypocenter depths have larger uncertainties. Downdip of the Nicoya Peninsula, it is ambiguous whether events at depths of 40 to 50 km are on the plate interface or within the plate. In this area, our preferred interpretation is that the downdip extent of microseismicity corresponds with the intersection of the Moho with the subducting plate. The downdip extent of microseismicity in southern Costa Rica correlates with the 150°C isotherm. A steeper plate subduction dip as suggested by A. Newman (verbal communication, 2010) would increase the plate interface temperatures in this region, as does frictional heating.

8. Conclusions

[57] We have numerically modeled the thermal regime of the Middle America Trench. We explored sensitivity to a number of models including those based on incoming oceanic crust

with a conductive geotherm and perturbed by hydrothermal circulation corresponding to both ventilated and insulated circulation using a Nusselt number approach [*Spinelli and Wang*, 2008]. In general, hydrothermal circulation warms the subduction thrust near the trench and cools the subduction thrust landward of the trench [*Kummer and Spinelli*, 2009].

[58] Comparisons between heat flow profiles across the margin and thermal models indicate that north of the plate suture heat flow data can be adequately fit by a cold geotherm with a ventilated style of circulation or a cold geotherm that conductively rebounds once the plate enters the subduction zone. South of the plate suture heat flow data is better fit by an intermediate geotherm in which hydrothermal circulation continues. Conductive reference models inadequately fit the heat flow data. Our preferred thermal models incorporate hydrothermal circulation within the subducting crust that results in a cooler subduction thrust than previous models [*Harris and Wang*, 2002; *Spinelli and Saffer*, 2004]. Comparisons between our thermal model of the subducting Cocos Plate and microseismicity along the subduction thrust show a good correlation between the 100°C isotherm and the updip limit of microseismicity. The downdip extent of microseismicity is presently ambiguous. These results show how differences in the incoming plate morphology and hydrology affect the thermal structure of the subduction zone.

Acknowledgments

[59] This research was support by an NSF award (OCE-0637120) to R. N. Harris. We thank R. von Huene, A. Newman, and P. Fulton for useful discussions. We thank an anonymous reviewer, Tim Minshull, and the Associate Editor for comments that clarified both our thinking and presentation. We thank K. Wang for the use of his thermal codes. Heat flow data acquisition was funded by the German Science Foundation (DFG) through grant Vi 133/7-1 to H.V. and I.G. and the SFB 574 "Volatiles and fluids in subduction zones" at Christan-Albrechts University, Kiel. This is a contribution of the Barcelona Center for Subsurface Imaging (Barcelona-CSI) supported by the Kaleidoscope project of REPSOL.

References

Barckhausen, U., C. R. Ranero, R. von Huene, S. C. Cande, and H. A. Roeser (2001), Revised tectonic boundaries in the Cocos Plate off Costa Rica; Implications for the segmentation of the convergent margin and for plate tectonic models, *J. Geophys. Res.*, *106*, 19,207–19,220, doi:10.1029/2001JB000238.

Bilek, S. L. (2007), Influence of subducting topography on earthquake rupture, in *The Seismogenic Zone of Subduction Thrust Faults*, edited by T. Dixon and C. Moore, pp. 123–146, Columbia Univ. Press, New York.

Bilek, S. L., S. Y. Schwartz, and H. R. DeShon (2003), Control of seafloor roughness on earthquake rupture behavior, *Geology*, *31*, 455–458, doi:10.1130/0091-7613(2003)031<0455:COSROE>2.0.CO;2.

Byerlee, J. D. (1978), Friction of rocks, *Pure Appl. Geophys.*, *116*, 615–626, doi:10.1007/BF00876528.

Byrne, T., and D. M. Fisher (1990), Evidence for a weak and overpressured decollement beneath sediment-dominated accretionary prisms, *J. Geophys. Res.*, *95*, 9081–9097, doi:10.1029/JB095iB06p09081.

Calahorrano, A., V. Sallarès, F. Sage, J.-Y. Collot, and C. R. Ranero (2008), Nonlinear variations of the physical properties along the Southern Ecuador subduction channel: Results from depth-migrated seismic data, *Earth Planet. Sci. Lett.*, *267*, 453–467, doi:10.1016/j.epsl.2007.11.061.

Caristan, Y. (1982), The transition from high temperature creep to fracture in Maryland diabase, *J. Geophys. Res.*, *87*, 6781–6790, doi:10.1029/JB087iB08p06781.

Christeson, G. L., K. D. McIntosh, T. H. Shipley, E. R. Flueh, and H. Goedde (1999), Structure of the Costa Rica convergent margin, offshore Nicoya Peninsula, *J. Geophys. Res.*, *104*, 25,443–25,468, doi:10.1029/1999JB900251.

Cloos, M. (1985), Thermal evolution of convergent plate margins: Thermal modeling and re-evaluation of isotopic Ar-ages for blueschists in the Fransican complex of California, *Tectonics*, *4*, 421–433, doi:10.1029/TC004i005p00421.

Currie, C. A., R. D. Hyndman, K. Wang, and V. Kostoglodov (2002), Thermal models of the Mexico subduction zone: Implications for the megathrust seismogenic zone, *J. Geophys. Res.*, *107*(B12), 2370, doi:10.1029/2001JB000886.

Dahlen, F. A., J. Suppe, and D. M. Davis (1984), Mechanics of fold-and-thrust belts and accretionary wedges: Cohesive coulomb theory, *J. Geophys. Res.*, *89*, 10,087–10,101, doi:10.1029/JB089iB12p10087.

Davis, E. E., K. Wang, J. He, D. S. Chapman, H. Villinger, and A. Rosenberger (1997), An unequivocal case for high Nusselt-number hydrothermal convection in sediment-buried igneous oceanic crust, *Earth Planet. Sci. Lett.*, *146*, 137–150, doi:10.1016/S0012-821X(96)00212-9.

DeMets, D. C. (2001), A new estimate for present-day Cocos-Caribbean plate motion: Implications for slip along the Central American volcanic arc, *Geophys. Res. Lett.*, *28*, 4043–4046, doi:10.1029/2001GL013518.

DeShon, H. R., S. Y. Schwartz, S. L. Bilek, L. M. Dorman, V. Gonzalez, J. M. Protti, E. R. Flueh, and T. H. Dixon (2003), Seismogenic zone structure of the southern Middle America Trench, Costa Rica, *J. Geophys. Res.*, *108*(B10), 2491, doi:10.1029/2002JB002294.

DeShon, H. R., S. Y. Schwartz, A. V. Newman, V. Gonzalez, M. Protti, L. M. Dorman, T. H. Dixon, D. E. Sampson, and E. R. Flueh (2006), Seismogenic zone structure beneath the Nicoya Peninsula, Costa Rica, from three-dimensional local earthquake P- and S-wave tomography, *Geophys. J. Int.*, *164*, 109–124, doi:10.1111/j.1365-246X.2005.02809.x.

Dixon, T. H., and J. C. Moore (Eds.) (2007), *The Seismogenic Zone of the Subduction Thrust Faults*, 680 pp., Columbia Univ. Press, New York.

Dumitru, T. A. (1991), Effects of subduction parameters on geothermal gradients in forearcs, with an application to Franciscan subduction in California, *J. Geophys. Res.*, *96*, 621–641, doi:10.1029/90JB01913.

Engdahl, E. R., R. van der Hilst, and R. Buland (1998), Global teleseismic earthquake relocation with improved travel times and procedures for depth determination, *Bull. Seismol. Soc. Am.*, *88*, 722–743.

Ferguson, I. J., G. K. Westbrook, M. G. Langseth, and G. P. Thomas (1993), Heat flow and thermal models of the Barbados ridge accretionary complex, *J. Geophys. Res.*, *98*, 4121–4142, doi:10.1029/92JB01853.

Fisher, A. T., C. A. Stein, R. N. Harris, K. Wang, E. A. Silver, M. Pfender, M. Hutnak, A. Cherkaoui, R. Bodzin, and H. Villinger (2003), Abrupt thermal transition reveals hydrothermal boundary and role of seamounts within the Cocos Plate, *Geophys. Res. Lett.*, *30*(11), 1550, doi:10.1029/2002GL016766.

Fisher, A. T., E. E. Davis, and K. Becker (2008), Borehole-to-borehole hydrologic response across 2.4 km in the upper oceanic crust: Implications for crustal-scale properties, *J. Geophys. Res.*, *113*, B07106, doi:10.1029/2007JB005447.

Ghosh, A., A. V. Newman, A. M. Thomas, and G. T. Farmer (2008), Interface locking along the subduction megathrust from *b*-value mapping near Nicoya Peninsula, Costa Rica, *Geophys. Res. Lett.*, *35*, L01301, doi:10.1029/2007GL031617.

Harris, R. N., and K. Wang (2002), Thermal models of the Middle America Trench at the Nicoya Peninsula, Costa Rica, *Geophys. Res. Lett.*, *29*(21), 2010, doi:10.1029/2002GL015406.

Harris, R. N., I. Grevemeyer, C. R. Ranero, H. Villinger, U. Barckhausen, T. Henke, C. Mueller, and S. Neben (2010), Thermal regime of the Costa Rican convergent margin: 1. Along-strike variations in heat flow from probe measurements and estimated from bottom-simulating reflectors, *Geochem. Geophys. Geosyst.*, doi:10.1029/2010GC003272, in press.

Harvey, A. H., A. P. Peskin, and S. A. Kline (1997), NIST/ASME steam properties, 49 pp., Natl. Inst. for Stand. and Technol., Gaithersburg, Md.

Heesemann, M., I. Grevemeyer, and H. Villinger (2009), Thermal constraints on the frictional conditions of the nucleation and rupture area of the 1992 Nicaragua tsunami earthquake, *Geophys. J. Int.*, *179*, doi:10.1111/j.1365-246X.2009.04187.x.

Hey, R. N. (1977), Tectonic evolution of the Cocos, Nazca spreading center, *Geol. Soc. Am. Bull.*, *88*, 1404–1420, doi:10.1130/0016-7606(1977)88<1404:TEOTCS>2.0.CO;2.

Hinz, K., R. von Huene, and C. R. Ranero (1996), Tectonic structure of the convergent Pacific margin offshore Costa Rica from multichannel seismic reflection data, *Tectonics*, *15*, 54–66.

Hippchen, S., and R. D. Hyndman (2008), Thermal and structural models of the Sumatra subduction zone: Implications for the megathrust seismogenic zone, *J. Geophys. Res.*, *113*, B12103, doi:10.1029/2008JB005698.

Husen, S., R. Quintero, E. Kissling, and B. Hacker (2003), Subduction-zone structure and magmatic processes constrained by local earthquake tomography and petrological modeling, *Geophys. J. Int.*, *155*, 11–32, doi:10.1046/j.1365-236X.2003.01984.x.

Hutnak, M., et al. (2007), The thermal state of 18–24 Ma upper lithosphere subducting below the Nicoya Peninsula, northern Costa Rica margin, in *The Seismogenic Zone of Subduction Thrust Faults*, edited by T. Dixon and C. Moore, pp. 86–122, Columbia Univ. Press, New York.

Hutnak, M., A. T. Fisher, R. Harris, C. Stein, K. Wang, G. Spinelli, M. Schindler, H. Villinger, and E. Silver (2008), Surprisingly large heat and fluid fluxes driven through mid-plate outcrops on ocean crust, *Nat. Geosci.*, *1*, 611–614, doi:10.1038/ngeo264.

Hyndman, R. D. (2007), The seismogenic zone of subduction thrust faults, in *The Seismogenic Zone of Subduction Thrust Faults*, edited by T. Dixon and C. Moore, pp. 15–40, Columbia Univ. Press, New York.

Hyndman, R. D., and K. Wang (1993), Thermal constraints on the zone of major thrust earthquakes failure: The Cascadia subduction zone, *J. Geophys. Res.*, *98*, 2039–2060, doi:10.1029/92JB02279.

Hyndman, R. D., M. Yamano, and D. A. Oleskevich (1997), The seismogenic zone of subduction thrust faults, *Isl. Arc*, *6*, 244–260, doi:10.1111/j.1440-1738.1997.tb00175.x.

Jaeger, J. C. (1964), Thermal effects of intrusions, *Rev. Geophys.*, *2*, 443–466, doi:10.1029/RG002i003p00443.

Kimura, G., et al. (1997), *Proceedings of the Ocean Drilling Program, Initial Reports*, vol. 170, Ocean Drill. Program, College Station, Tex.

Kummer, T., and G. A. Spinelli (2008), Hydrothermal circulation in subducting crust reduces subduction zone temperatures, *Geology*, *36*, 91–94, doi:10.1130/G24128A.1.

Kummer, T., and G. A. Spinelli (2009), Thermal effects of fluid circulation in the basement aquifer of subducting oceanic crust, *J. Geophys. Res.*, *114*, B03104, doi:10.1029/2008JB006197.

Langseth, M. G., and E. A. Silver (1996), The Nicoya convergent margin—A region of exceptionally low heat flow, *Geophys. Res. Lett.*, *23*, 891–894, doi:10.1029/96GL00733.

Lay, T., and S. L. Bilek (2007), Anomalous earthquake ruptures at shallow depths on subduction zone megathrusts, in *The Seismogenic Zone of Subduction Thrust Faults*, edited by T. Dixon and C. Moore, pp. 476–511, Columbia Univ. Press, New York.

MacKenzie, L., G. A. Abers, K. M. Fischer, E. M. Syracuse, J. M. Protti, and W. Strauch (2008), Crustal structure along the southern Central American volcanic front, *Geochem. Geophys. Geosyst.*, *9*, Q08S09, doi:10.1029/2008GC001991.

Marone, C., and D. M. Saffer (2007), Fault friction and the upper transition from seismic to aseismic faulting, in *The Seismogenic Zone of Subduction Thrust Faults*, edited by T. H. Dixon and J. C. Moore, pp. 346–369, Columbia Univ. Press, New York.

Molnar, P., and P. England (1995), Temperatures in zones of steady-state underthrusting of young oceanic lithosphere, *Earth Planet. Sci. Lett.*, *131*, 57–70, doi:10.1016/0012-821X(94)00253-U.

Moore, J. C., and D. Saffer (2001), Updip limit of the seismogenic zone beneath the accretionary prism of southwest Japan: An effect of diagenetic to low-grade metamorphic processes and increasing effective stress, *Geology*, *29*, 183–186, doi:10.1130/0091-7613(2001)029<0183:ULOTSZ>2.0.CO;2.

Newman, A. V., S. Y. Schwartz, V. Gonzalez, H. R. DeShon, J. M. Protti, and L. M. Dorman (2002), Along-strike variability in the seismogenic zone below Nicoya Peninsula, Costa Rica, *Geophys. Res. Lett.*, *29*(20), 1977, doi:10.1029/2002GL015409.

Oleskevich, D. A., R. D. Hyndman, and K. Wang (1999), The updip and downdip limits to great subduction earthquakes: Thermal and structural models of Cascadia, south Alaska, SW Japan, and Chile, *J. Geophys. Res.*, *104*, 14,965–14,991, doi:10.1029/1999JB900060.

Peacock, S. M., and R. D. Hyndman (1999), Hydrous minerals in the mantle wedge and the maximum depth of subduction

thrust earthquakes, *Geophys. Res. Lett.*, *26*, 2517–2520, doi:10.1029/1999GL900558.

Peacock, S. M., and K. Wang (1999), Seismic consequences of warm versus cool subduction metamorphism: Examples from southwest and northeast Japan, *Science*, *286*, 937–939.

Peacock, S. M., P. E. Van Keken, S. D. Holloway, B. R. Hacker, G. A. Abers, and R. L. Fergason (2005), Thermal structure of the Costa Rica–Nicaragua subduction zone, *Phys. Earth Planet. Inter.*, *149*, 187–200, doi:10.1016/j.pepi.2004.08.030.

Peng, Z., and J. Gomberg (2010), An integrated perspective of the continuum between earthquakes and slow-slip phenomena, *Nat. Geosci.*, *3*, 599–607, doi:10.1038/NGEO0940.

Pindell, J. L., and S. F. Barrett (1990), Geologic evolution of the Caribbean: A plate-tectonic perspective, in *The Geology of North America*, vol. H, *The Caribbean Region*, edited by G. Dengo and J. E. Case, pp. 405–432, Geol. Soc. of Am., Boulder, Colo.

Protti, M., F. Guendal, and K. McNally (1995), Correlation between the age of the subducting Cocos plate and the geometry of the Wadati-Benioff zone under Nicaragua and Costa Rica, in *Geologic and Tectonic Development of the Caribbean Plate Boundary in Southern Central America*, edited by P. Mann, *Spec. Pap. Geol. Soc. Am.*, *295*, 309–326.

Ranero, C. R., and R. von Huene (2000), Subduction erosion along the Middle America convergent margin, *Nature*, *404*, 748–752, doi:10.1038/35008046.

Ranero, C. R., J. Phipps Morgan, K. McIntosh, and C. Reichert (2003), Bending-related faulting and mantle serpentinization at the Middle America Trench, *Nature*, *425*, 367–373, doi:10.1038/nature01961.

Ranero, C. R., A. Villaenor, J. Phipps Morgan, and W. Weinrebe (2005), Relationship between bend-faulting at trenches and intermediate-depth seismicity, *Geochem. Geophys. Geosyst.*, *6*, Q12002, doi:10.1029/2005GC000997.

Ranero, C. R., R. von Huene, W. Weinrebe, and U. Barckhausen (2007), Convergent margin tectonics of Middle America: A marine perspective, in *Central America: Geology, Resources and Hazards*, edited by J. Bunschuh and G. E. Alvarado, pp. 239–265, Taylor and Francis, London.

Ranero, C. R., I. Grevemeyer, H. Sahling, U. Barchkhausen, C. Hensen, K. Wallmann, W. Weinrebe, P. Vannucchi, R. von Huene, and K. McIntosh (2008), Hydrogeological system of erosional convergent margins and its influence on tectonics and interplate seismogenesis, *Geochem. Geophys. Geosyst.*, *9*, Q03S04, doi:10.1029/2007GC001679.

Ruppel, C., and M. Kinoshita (2000), Fluid, methane, and energy flux in an active margin gas hydrate province, offshore Costa Rica, *Earth Planet. Sci. Lett.*, *179*, 153–165, doi:10.1016/S0012-821X(00)00096-0.

Sage, F., J. Y. Collot, and C. R. Ranero (2006), Interplate patchiness and subduction-erosion mechanisms: Evidence from depth-migrated seismic images at the central Ecuador convergent margin, *Geology*, *34*(12), 997–1000, doi:10.1130/G22790A.1.

Sallarès, V., J. J. Dañobeitia, and E. R. Flueh (2000), Seismic tomography with local earthquakes in Costa Rica, *Tectonophysics*, *329*, 61–78, doi:10.1016/S0040-1951(00)00188-8.

Sallarès, V., J. J. Dañobeitia, and E. R. Flueh (2001), Lithospheric structure of the Costa Rican Isthmus: Effects of subduction zone magmatism on an oceanic plateau, *J. Geophys. Res.*, *106*, 621–643, doi:10.1029/2000JB900245.

Satake, K. (1994), Mechanism of the 1992 Nicaragua tsunami earthquake, *Geophys. Res. Lett.*, *21*(23), 2519–2522, doi:10.1029/94GL02338.

Schwartz, S. Y., and H. R. DeShon (2007), Distinct updip limits to geogetic locking and microseismicity at the northern Costa Rica seismogenic zone: Evidence for two mechanical transitions, in *The Seismogenic Zone of Subduction Thrust Faults*, edited by T. Dixon and C. Moore, pp. 576–599, Columbia Univ. Press, New York.

Schwartz, S. Y., and J. M. Rokosky (2007), Slow slip events and seismic tremor at circum-Pacific subduction zones, *Rev. Geophys.*, *45*, RG3004, doi:10.1029/2006RG000208.

Seno, T. (2005), Variation of downdip limit of the seismogenic zone near the Japanese islands: Implications for the serpentinization mechanism of the forearc mantle wedge, *Earth Planet. Sci. Lett.*, *231*, 249–262, doi:10.1016/j.epsl.2004.12.027.

Silver, E., P. Costa Pisani, M. Hutnak, A. Fisher, H. DeShon, and B. Taylor (2004), An 8–10 Ma tectonic event on the Cocos Plate offshore Costa Rica: Result of Cocos Ridge collision, *Geophys. Res. Lett.*, *31*, L18601, doi:10.1029/2004GL020272.

Sinton, C. W., R. A. Duncan, and P. Cenyer (1997), Nicoya Peninsula, Costa Rica: A single suite of Caribbean oceanic plateau magmas, *J. Geophys. Res.*, *102*, 15,507–15,520, doi:10.1029/97JB00681.

Spinelli, G. A., and D. M. Saffer (2004), Along-strike variations in underthrust sediment dewatering on the Nicoya margin, Costa Rica related to the updip limit of seismicity, *Geophys. Res. Lett.*, *31*, L04613, doi:10.1029/2003GL018863.

Spinelli, G. A., and K. Wang (2008), Effects of fluid circulation in subducting crust on Nankai margin seismogenic zone temperatures, *Geology*, *36*, 887–890, doi:10.1130/G25145A.1.

Spinelli, G. A., and K. Wang (2009), Links between fluid circulation, temperature, and metamorphism in subducting slabs, *Geophys. Res. Lett.*, *36*, L13302, doi:10.1029/2009GL038706.

Spinelli, G. A., D. M. Saffer, and M. B. Underwood (2006), Hydrogeologic responses to three-dimensional temperature variability, Costa Rica subduction margin, *J. Geophys. Res.*, *111*, B04403, doi:10.1029/2004JB003436.

Stavenhagen, A. U., E. R. Flueh, C. Ranero, K. D. McIntosh, T. Shipley, G. Leandro, A. Schultze, and J. J. Dañobeitia (1998), Seismic wide-angle investigations in Costa Rica—A crustal velocity model from the Pacific to the Caribbean, *Zentralbl. Geol. Palaeontol., Teil 1*, *3*, 393–408.

Stein, C., and S. Stein (1992), A model for the global variation in oceanic depth and heat flow with lithospheric age, *Nature*, *359*, 123–129, doi:10.1038/359123a0.

Syracuse, E. M., G. A. Abers, K. Fischer, L. MacKenzie, C. Rychert, M. Protti, V. Gonzalez, and W. Strauch (2008), Seismic tomography and earthquake locations in the Nicaraguan and Costa Rican upper mantle, *Geochem. Geophys. Geosyst.*, *9*, Q07S08, doi:10.1029/2008GC001963.

Underwood, M. B. (2007), Sediment inputs to subduction zones: Why lithostratigraphic and clay mineralogy matter, in *The Seismogenic Zone of Subduction Thrust Faults*, edited by T. Dixon and C. Moore, pp. 42–85, Columbia Univ. Press, New York.

Vacquier, V., J. G. Sclater, and C. E. Corry (1967), Studies in the thermal state of the earth, the 21st paper: Heat-flow, eastern Pacific, *Bull. Earthquake Res. Inst.*, *45*, 375–393.

van den Beukel, J., and R. Wortel (1988), Thermo-mechanical modeling of arc-trench regions, *Tectonophysics*, *154*, 177–193, doi:10.1016/0040-1951(88)90101-1.

Von Herzen, R., and S. Uyeda (1963), Heat flow through the eastern Pacific floor, *J. Geophys. Res.*, *68*, 4219–4250.

von Huene, C. R., and C. R. Ranero (2003), Subduction erosion and basal friction along the sediment-starved convergent margin off Antofagasta, Chile, *J. Geophys. Res.*, *108*(B2), 2079, doi:10.1029/2001JB001569.

von Huene, R., et al. (1995), Morphotectonics of the Pacific convergent margin of Costa Rica, Geologic and tectonic development of the Caribbean plate boundary, in *Southern Central America*, edited by P. Mann, *Spec. Pap. Geol. Soc. Am.*, *295*, 291–307.

von Huene, R., C. R. Ranero, W. Weinrebe, and K. Hinz (2000), Quaternary convergent margin tectonics of Costa Rica, segmentation of the Cocos Plate, and Central America volcanism, *Tectonics*, *19*, 314–334, doi:10.1029/1999TC001143.

von Huene, R., C. R. Ranero, and D. W. Scholl (2009), Convergent margin structure in high-quality geophysical images and current kinematic and dynamic models, in *Subduction Zone Dynamics*, edited by S. Lallemand and F. Funiciello, pp. 137–157, doi:10.1007/978-3-540-87974-9_8, Springer, Berlin.

Vrolijk, P. (1990), On the mechanical role of smectite in subduction zones, *Geology*, *18*, 703–707, doi:10.1130/0091-7613(1990)018<0703:OTMROS>2.3.CO;2.

Walther, C. H. E. (2003), The crustal structure of the Cocos ridge off Costa Rica, *J. Geophys. Res.*, *108*(B3), 2136, doi:10.1029/2001JB000888.

Wang, K., and J. He (1999), Mechanics of low-stress forearcs: Nankai and Cascadia, *J. Geophys. Res.*, *104*, 15,191–15,205, doi:10.1029/1999JB900103.

Wang, K., T. Mulder, G. C. Rogers, and R. D. Hyndman (1995), Case for very low coupling stress on the Cascadia subduction fault, *J. Geophys. Res.*, *100*, 12,907–12,918, doi:10.1029/95JB00516.

Werner, R., K. Hoernle, P. van den Bogaard, C. Ranero, and R. von Huene (1999), Drowned 14-m.y.-old Galapagos archipelago off the coast of Costa Rica: Implications for tectonic and evolutionary models, *Geology*, *27*, 499–502, doi:10.1130/0091-7613(1999)027<0499:DMYOGP>2.3.CO;2.

Ye, S., J. Bialas, E. R. Flueh, A. Stavenhagen, R. von Huene, G. Leandro, and K. Hinz (1996), Crustal structure of the Middle America Trench off Costa Rica from wide-angle seismic data, *Tectonics*, *15*, 1006–1021, doi:10.1029/96TC00827.